Flux and turbulence measurements at a densely built-up site in Marseille: Heat, mass (water and carbon dioxide), and momentum

C. S. B. Grimmond,[1] J. A. Salmond,[2] T. R. Oke,[3] B. Offerle,[1] and A. Lemonsu[4]

Received 20 April 2004; revised 15 September 2004; accepted 30 September 2004; published 16 December 2004.

[1] Eddy covariance (EC) observations above the densely built-up center of Marseille during the Expérience sur site pour contraindre les modèles de pollution atmosphérique et de transport d'émissions (ESCOMPTE) summertime measurement campaign extend current understanding of surface atmosphere exchanges in cities. The instrument array presented opportunities to address issues of the representativeness of local-scale fluxes in urban settings. Separate EC systems operated at two levels, and a telescoping tower allowed the pair to be exposed at two different sets of heights. The flux and turbulence observations taken at the four heights, stratified by wind conditions (mistral wind and sea breeze), are used to address the partitioning of the surface energy balance in an area with large roughness elements. The turbulent sensible heat flux dominates in the daytime, although the storage heat flux is a significant term that peaks before solar noon. The turbulent latent heat flux is small but not negligible. Carbon dioxide fluxes show that this central city district is almost always a source, but the vegetation reduces the magnitude of the fluxes in the afternoon. The atmosphere in such a heavily developed area is rarely stable. The turbulence characteristics support the empirical functions proposed by M. Roth. *INDEX TERMS:* 0315 Atmospheric Composition and Structure: Biosphere/atmosphere interactions; 0345 Atmospheric Composition and Structure: Pollution—urban and regional (0305); 1803 Hydrology: Anthropogenic effects; 3307 Meteorology and Atmospheric Dynamics: Boundary layer processes; 3322 Meteorology and Atmospheric Dynamics: Land/atmosphere interactions; *KEYWORDS:* carbon dioxide fluxes, eddy covariance, energy balance, stability, turbulence, urban climate

Citation: Grimmond, C. S. B., J. A. Salmond, T. R. Oke, B. Offerle, and A. Lemonsu (2004), Flux and turbulence measurements at a densely built-up site in Marseille: Heat, mass (water and carbon dioxide), and momentum, *J. Geophys. Res.*, *109*, D24101, doi:10.1029/2004JD004936.

1. Introduction

[2] At the end of the twentieth century, approximately half of the world's population, over three billion people, lived in urban areas. By 2025, the United Nations (cited by *Uitto and Biswas* [2000]) predicts that this number will double, and that two thirds of the global population will live in urban areas. Alteration of the land surface and atmosphere by urban development leads to the creation of distinct urban climates. Ultimately, these urban climate effects are due to differences in the exchanges of heat, mass, and momentum between the city and its preexisting landscape. Thus the understanding, prediction, and mitigation of urban climate effects are intricately tied to knowledge of surface-atmosphere exchanges in urban environments.

[3] Urban areas comprise a wide range of land covers and land uses. This diversity presents a multiplicity of boundary conditions to the atmosphere. These include controls exerted by roughness (the size, shape and separation of buildings and vegetation), the radiative, thermal, and moisture properties of all facets of the urban system and their spatial arrangement, and patterns of emissions (carbon dioxide, for example). In any given urban area these properties are organized uniquely because of the particular blend of topography, climate, economy, history and culture, and the residential, industrial and commercial land uses that differentiate its districts. Recognition of this has directed research to understand the spatial and temporal variability of surface-atmosphere exchanges within and between cities, within and between land uses, and the causes that underlie such differences. Several studies have been conducted in North American cities, mainly in summertime conditions and residential neighborhoods (see summary given by *Grimmond and Oke* [2002]). More recently, flux observations have been conducted outside of North America; see, for example, work in Christchurch, New Zealand [*Spronken-Smith*, 2002], and Tokyo, Japan [*Moriwaki and Kanda*, 2004]. Studies in European cities add significantly new characteristics to the mix because of these cities' distinct architectural styles, building materials, climatic

[1]Atmospheric Science Program, Department of Geography, Indiana University, Bloomington, Indiana, USA.
[2]School of Geography, Earth and Environmental Sciences, University of Birmingham, Birmingham, UK.
[3]Department of Geography, University of British Columbia, Vancouver, British Columbia, Canada.
[4]Centre National de Recherches Meteorologiques, Météo France, Toulouse, France.

0148-0227/04/2004JD004936$09.00

settings and energy use/emission patterns (for example, Zurich, Switzerland [*Rotach*, 1995]; Basel, Switzerland [*Feigenwinter et al.*, 1999; *Christen et al.*, 2002]; Edinburgh, Scotland [*Nemitz et al.*, 2002]; and Łódź, Poland [*Offerle et al.*, 2004]). There are also examples of longer-term studies encompassing at least the full seasonal cycle and even multiple years [*Anderson and Taggart*, 2002; *Christen et al.*, 2002; *Grimmond et al.*, 2002b; *Moriwaki and Kanda*, 2004; *Offerle et al.*, 2004]. Collectively, these studies document the temporal and spatial variability of flux partitioning, both within and between urban areas. Nevertheless, the range of conditions studied, both in terms of meteorology (seasonal and synoptic conditions) and surface cover (building sizes, shapes and arrangements, and vegetation cover) remains limited, especially compared with the many studies of surface-atmosphere fluxes in forested, agricultural, wetland, snow and ice environments.

[4] In June–July 2001, a multidisciplinary study of urban air pollution, the Expérience sur site pour contraindre les modèles de pollution atmosphérique et de transport d'émissions (ESCOMPTE) project, was conducted in the Berre-Marseille region, of France [*Cros et al.*, 2004; *Mestayer et al.*, 2004]. As part of this extensive study, local-scale fluxes of heat, mass, momentum, and carbon dioxide were measured at a central city site in Marseille. These flux data provide information on the summertime surface energy balance and carbon dioxide fluxes in a densely built-up area (little vegetation, tall buildings with massive walls and deep street canyons) under a range of wind conditions (strong mistral winds and sea breezes). The instrument configuration made it possible to address the representativeness of local-scale fluxes in such a district because two sets of instruments were operated at two sets of heights. Moreover, the availability of complementary observations of surface temperature [*Pigeon et al.*, 2002; *Roberts et al.*, 2003; *Lagouarde et al.*, 2004], spatially integrated sensible heat fluxes [*Irvine et al.*, 2002; *Lagouarde et al.*, 2002], boundary layer structure [*Mestayer et al.*, 2004], and the results of detailed numerical modeling [*Lemonsu et al.*, 2004a, 2004b] provide independent data against which to evaluate and interpret the local-scale flux data.

2. Methods

2.1. The City

[5] Marseille, the second largest city in France, is a major seaport and an industrial and commercial center. Its current population exceeds 800,000; more than two million people live in the extended metropolitan area. Marseille is located at the south end of the Rhône Valley, a long north-south rift between the Cévenne Mountains and the foothills of the French Alps. The city itself is surrounded by hills, 400–650 m in height, separated by small valleys that channel flow toward the city center. The Gulf of Lyons is located directly to the west of the city, and the open Mediterranean Sea lies approximately 10 km to the south.

2.2. The Site

2.2.1. Urban Structure and Roughness

[6] The measurement site, centered on the Cour d'appel administratif (CAA, ESCOMPTE site E10), is located at 43°17′N, 5°23′E (elevation 70 m asl), in a dense commercial and residential area of the city (Figure 1). Buildings are 4–6 stories in height with an average height (z_H) of 15.6 m (Table 1), based on a ground survey and analysis of the *Long et al.* [2002] database near the site. Vegetation is largely contained within the urban canyons or inner courtyards. The zero-plane displacement length (z_d), based on rule-of-thumb estimates (where $z_d = 0.7\ z_H$ [*Grimmond and Oke*, 1999a]), is ~11 m. Using this value for z_d and the log law, we estimate the roughness length for momentum (z_0) for the site is ~2.5 m.

2.2.2. Surface Cover

[7] On the basis of visual analysis of a color aerial photographic image (provided by M.-A. Velay-Dabat, Laboratoire ABC, Ecole d'Architecture de Marseille-Luminy), information on the surface cover and materials around the site was generated for an area of 3.5 km (north-south) × 2.5 km (east-west). The surface cover was classified into 15 types (Table 2). This information was combined with building height data (based on the 2 m resolution database of *Long et al.* [2002] derived from data of the Institut Géographique National de France (IGN)), to generate a 10 m × 10 m resolution database of surface materials and morphometry (for details, see *Lemonsu et al.* [2004a] and *Mestayer et al.* [2004]).

[8] To determine the surface characteristics affecting the flux observations for any 60 min period, the flux source area model (FSAM) of *Schmid* [1994] was used to estimate the source areas of the turbulent fluxes. Given the limits of FSAM, the range of the stability conditions encountered during the study period (see section 3.8) and the height of the sensors relative to the roughness elements, source area could not be estimated for some observations. However, it is possible to estimate the probable characteristics of the source areas for most observation periods. The three inputs to the FSAM model are related to stability ($z'/L = [z_s - z_d]/L$, where z_s is the sensor height and L is Obukhov length) (see section 3.8), sensor height ($[z_s - z_d]/z_0$), and lateral turbulence characteristics (σ_v/u^* where σ_v is the standard deviation of the lateral velocity and u* is the friction velocity). The size of the source area increases with increasing sensor height; its length increases as atmospheric stability changes from unstable to neutral to stable conditions; and its width increases with σ_v/u^*. For those times when FSAM did not yield a result, a source area filter was assigned on the basis of results for periods with the closest meteorological conditions for the 60 min period.

[9] Source weights for each grid square were used to calculate the appropriate surface characteristics influencing each 60 min flux observation from a GIS database. The composite daytime source areas during mistral and sea breeze conditions are given by *Lemonsu et al.* [2004a] (their Figure 10).

2.3. Micrometeorological Measurements

[10] The micrometeorological instrumentation at the CAA site (Table 3) was mounted on a pneumatic mast (Hilomast NX30) installed on the roof of the building. The base of the tower was 20.7 m above ground level. Equipment was mounted at two levels (L1 upper and L2 lower) on the tower (Table 4). The tower was operated in two modes: up (U) when the tower was extended to its greatest height of operation and down (D) when the tower

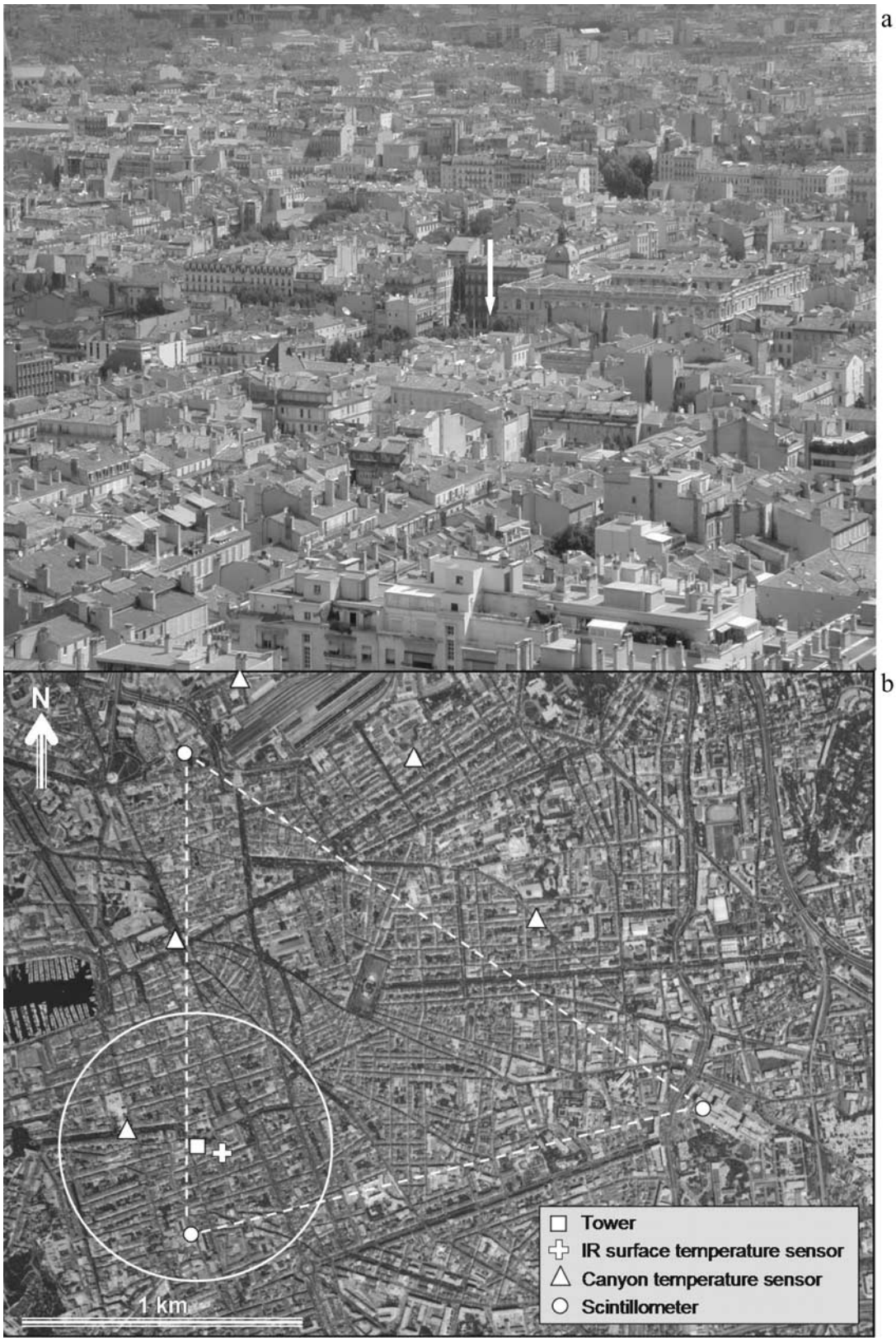

Figure 1. Images of the study site: (a) Oblique photograph looking north showing the observation site. Arrow indicates location of tower. (b) Aerial photograph of city center with location of the tower and other sensors. The horizontal bar is 1 km. Note that this is a modified version of Figure 1 of *Lemonsu et al.* [2004a], which had errors. See color version of this figure in the HTML.

Table 1. Surface Characteristics of the Study Site[a]

Surface Property	Value
Albedo (D1)	0.18
Albedo (U1)	0.16
Sky view factor (mean)	0.40
Roughness length	2.5 m
Zero-plane displacement length	11 m
Mean building height, z_H	15.6 m
Mean surface fraction vegetated (when at U1, D1)	0.11, 0.14

[a]See text for further explanation of methods used to obtain values. Sky view factor calculated using a digital camera and methods described by *Grimmond et al.* [2001] at ~1.5 m.

was partially retracted because of strong wind conditions. Thus at any given time the two eddy covariance (EC) systems, vertically separated by 6 m, operated in one of these two modes, depending on wind conditions (Table 4). The mast was located along the path of a large aperture scintillometer. Thus fluxes measured at the tower using eddy covariance techniques can be compared with those measured along the scintillometer path [*Lagouarde et al.*, 2004; *Lemonsu et al.*, 2004a].

[11] The methods used to acquire and process the meteorological data are similar to those described by *Schmid et al.* [2000] and *Offerle et al.* [2004]. Two sonic anemometers (RM Young, Model 81000) were used to measure the three-dimensional (3-D) wind velocities (u, v, w) and virtual air temperature (T). Two infrared gas analyzers (Licor, Model 7500) were used to measure fluctuations of water vapor and carbon dioxide. A net radiometer (Kipp and Zonen, Model CNR1) measured the incoming (↓) and outgoing (↑) shortwave (K) and longwave (L) radiation fluxes. All instruments (Table 3), except for the sonic anemometers (SAT), were wired to a datalogger (Campbell Scientific 23X). The SATs were connected directly to the serial ports of a computer. The signals for the eddy covariance calculations were sampled at 10 Hz, and data were subjected to spike detection and rejection algorithms. The lag between the sonic measurements and the IRGA was set to the lag of maximum correlation between the thermocouple and the sonic temperature over the flux-averaging interval. Following *Kaimal and Finnigan* [1994], the variances and covariances are rotated to streamwise coordinates for flux computation. At hourly intervals, Q_H, Q_E and turbulence statistics are computed, and block averages are used to compute the instantaneous fluctuations. Corrections were applied for sonic virtual temperature [*Schotanus et al.*, 1983] and the density correction [*Webb et al.*, 1980] for Q_E and F_{CO2}. All data (raw and calculated statistics) are subjected to strict data limits to reject implausible values. All data are referred to in terms of local time.

Table 2. Surface Cover/Materials Mapped Visually From Color Aerial Photographs[a]

General Class	Materials Categorized
Roofs	tile roofs, metal roofs, gravel roofs, white roofs, green roofs, black roofs
Impervious	roads, concrete courtyards, railway
Water	harbor, fountains, boats
Vegetation	trees, other (mainly grass), bare ground

[a]A portion of the image is shown in Figure 1b.

Table 3. Instrumentation Used at the CAA Site (ESCOMPTE Site E10)[a]

Variable	Instrument	Model	Level
u, v, w, u*, Q_H, T, τ	sonic anemometer	RM Young 81000	L1, L2
CO_2, H_2O	infrared gas analyzer	Licor-7500	L1, L2
K↓, K↑, L↓, L↑, Q*	radiometer	Kipp & Zonen CNR1	L1
T	thermocouple	Omega T-type 36 awg	nine heights
T, RH	T/RH sensor	Vaisala HMP35C with Gill radiation shield	L2
Surface moisture		Weiss-type	
Surface T	infrared radiation thermometer	Everest, various	

[a]See text for definition of variables. Levels and their heights are defined in Table 4.

[12] Rotation of the coordinate system of the 3-D turbulence data, particularly the vertical component, has been much discussed in the micrometeorological literature [*Lee*, 1998; *Paw U et al.*, 2000; *Wilczak et al.*, 2001; *Massman and Lee*, 2002; *Finnigan et al.*, 2003; *Su et al.*, 2004]. Most recently, the use of a planar fit method is recommended [*Paw U et al.*, 2000; *Baldocchi et al.*, 2001; *Wilczak et al.*, 2001]. However, in this study since we do not have a long-term record of flux observations, the influence of tilt and flow distortion on the mean vertical velocity ($\bar{w}$) cannot be determined easily (given the need for the assumption that $\bar{w}$ is zero over "long" periods). Here this issue is exacerbated because the instruments were not kept at the same position at all times (the mode of operation of the tower and thus the height of the instruments varied). Therefore the data set would need to be divided into short periods for analysis, resulting in inadequate data for a range of wind directions. Thus we chose to report flux data without planar coordinate rotation. The implication is that local topographic effects have not been removed.

2.4. Meteorological Conditions During the Observation Period

[13] Measurements were undertaken from 16 June 2001 (day 167) to 14 July 2001 (day 195). The reference climate station for this area, which is part of the Global Station Network, is Marseille-Marignane (World Meteorological Organization (WMO) ID 07650), located at 43°45′N, 5°23′E (elevation 36 m asl) (WMO, GSN stations list region 6 Europe, http://www.wmo.ch/web/gcos/region6europe.htm, 2002). Data from this station are available from 1921 to 1999 from *National Climatic Data Center* [2002]. On the basis of these data, climatologically the June–July period is the driest period of the year (Figure 2). July has the highest average surface pressures and the warmest temperatures. June 2001 was drier than usual. In the study period it only

Table 4. Heights at Which EC Equipment Was Operated[a]

	L1	L2	z_{L1}/z_H	z_{L2}/z_H
Up	43.9 m (U1)	37.9 m (U2)	2.81	2.42
Down	34.6 m (D1)	28.5 m (D2)	2.22	1.83

[a]"L" refers to level, and "up" and "down" refer to the height to which the tower was extended; z_H is the average height of the buildings. The radiation equipment was mounted at level 1 (L1).

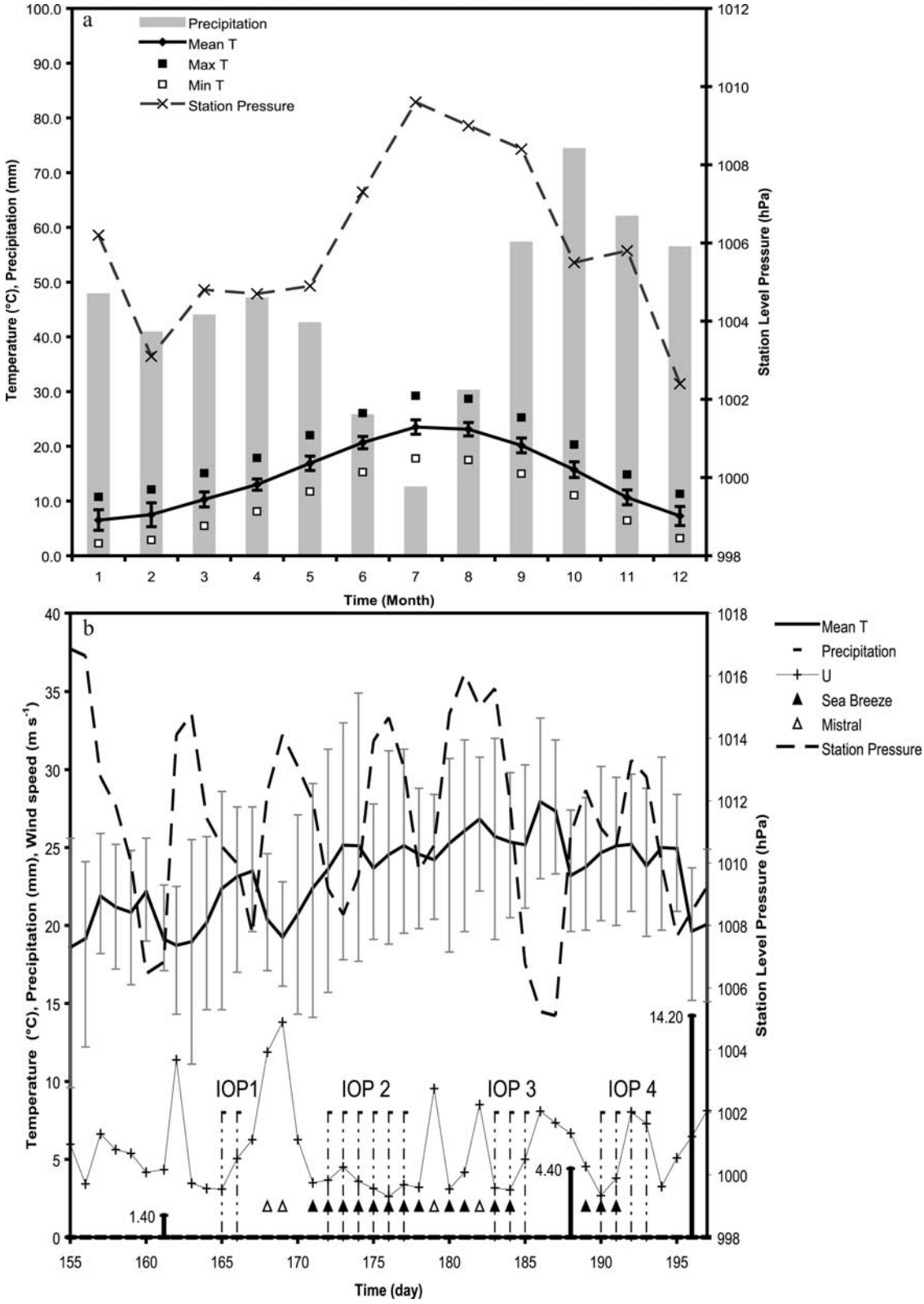

Figure 2. (a) Average climatology by month for Marseille-Marignane (WMO ID 07650) based on WMO Global Station Network (1921–1999) data. Mean and standard deviation are shown for temperature (T) and precipitation along with mean, maximum, and minimum temperature and station level pressure. (b) Conditions at Marseille-Marignane during ESCOMPTE, times of intensive operation periods (IOPs), and wind régime classification (see text) are shown. Days without a symbol are classified as ''other.'' Bars associated with the mean temperature are the maximum and minimum temperatures for the day.

rained twice with the most significant rain occurring at the end of the field campaign (Figure 2b). Through the study period, the characteristic sequence of synoptic conditions involved rising atmospheric pressure followed by lower pressure every 5–6 days.

[14] Much of the observation of surface-atmosphere fluxes in cities has been restricted to places with low wind speeds. An exception is Tucson, where simple parameterization schemes that work well elsewhere perform more poorly [*Grimmond and Oke*, 2002]. Therefore, in Marseille, where strong winds were common, the effect of wind on local-scale flux partitioning was of particular interest. In order to facilitate this analysis, G. Pigeon (Météo France, personal communication, 2001) classified each day of the study period into one of three wind régimes (''mistral,'' ''sea breeze,'' and ''other'') using wind speed and direction data from the station Vallon Dol (see location in Figure 1 of *Mestayer et al.* [2004]). The mistral is a strong NW katabatic wind (>7 m s^{-1}) that emerges from the Rhône Valley and is driven primarily by synoptic-scale pressure differences between the Pyrénées and the Apennines. Mistral events are most common during winter and spring. The mistral often develops after midnight, or in the early hours of the morning. Once established, however, the wind speeds associated with the mistral generally peak in the afternoon, weakening in the evening. Typically, mistral conditions prevail for 1–3 days, occasionally lasting a full week. In contrast, sea breeze flow has light to moderate winds from the NW, SW or SE. This range of directions is a response to the complex geometry of the coastline around Marseille, which means that the sea breeze front moves onshore from several directions. The category ''other'' includes those days where there is a large variation in wind direction and speed. Under these conditions, winds tend to be light during the night and morning (<5 m s^{-1}). The wind conditions on any given day are shown in Figure 2b.

3. Results and Discussion

[15] Turbulence data were collected from four levels (two at any given time) and radiation at two levels (one at any time) (Table 4). Stratifying the data by level and wind direction allowed the influence of surface cover on flux partitioning and of the representativeness of surface-atmosphere fluxes to be studied. The influence of the height of the measurements is considered first, then the effect of the different wind régimes and surface properties on the fluxes are discussed.

3.1. Effects of Wind Régimes

[16] As a precursor to this analysis, it is useful to consider the actual wind conditions observed during the study period and their diurnal pattern. To study the effects of changes in wind direction, the data were stratified into 60° sectors: Dir 1 from 0° to 60°; Dir 2 from 60° to 120°, etc. Mean values for a direction are reported only if there was a minimum of four 60 min samples for that direction. When the tower is in the U position, data from the uppermost instrument level exhibit a greater range of wind directions. In contrast when the tower in the D position winds were predominately from the west-north sectors. This is expected since the tower was retracted to the lower (D) position when strong mistral winds were forecast. Overall, the highest mean wind speeds (average 6.5 m s^{-1}) occurred in the afternoon from direction 6 (300°–360°) when the tower was in position D1. Although the tower is lower, the results are consistent with what was expected under the influence of the mistral.

3.2. Effects of Measurement Height

[17] The nature of the vertical structure of the atmosphere in urban areas is of interest both from the perspective of measurement and modeling [*Rotach et al.*, 2002]. The presence of large roughness elements in cities means the roughness sublayer is large relative to the inertial sublayer, or constant flux layer. This has implications for the height of instrument exposure to ensure measurements are representative of the appropriate spatial scale. Instruments located within the surface layer above the blending height (or the roughness sublayer), where the differences from the microscale variability have been smoothed out or integrated, can be considered representative local-scale measurements. Below this height, measurements are affected by the microscale effects of individual elements and surfaces and show enhanced variability in space and time [*Oke*, 1997; *Rotach*, 1999; *Roth*, 2000; *Rotach et al.*, 2002]. On the basis of wind tunnel observations, *Kastner-Klein and Rotach* [2004] show that at heights above approximately 2 times the mean height of the roughness elements (z_H) this transition should occur (see their Figure 5). It has been suggested that the multiple may, however, depend on the density of the element spacing: least at high, and greatest at low, densities [*Oke*, 2004].

[18] To investigate the height of the transition in Marseille, observations of Q_H and u* from the two levels of instrumentation (L1 and L2) were compared when the tower was in the up and down modes (Table 4). The ratio of the sensor data (L1/L2) for 60 min periods were calculated and stratified by tower position (U and D) and time of day. When the tower is in position U, during the day the ratio of u* values for the two heights is close to unity (Figure 3); that is, u* from both levels of EC instruments on the tower are similar. In contrast, when the tower is in the D position (and the lower instrument package is mounted below 2 z_H) measurements of u* differ. Values from the lower level are consistently less than those at the upper level, hence the ratio is greater than unity. Broadly similar results are evident for the observed sensible heat fluxes. When the tower is extended (U) both instrument levels record similar fluxes (Figure 3), but when retracted (D), the lower instruments (D2) measure lower Q_H. Greater variability is evident for both u* and Q_H at night. This is not surprising given that ratios of small values are involved, and wind velocities are less giving greater measurement error [*Baldocchi et al.*, 2001].

[19] When the ratio of u* or Q_H for the two levels is close to unity, we conclude that both sets of instruments are within the constant flux layer. At this site, therefore, when the tower is in the U position, and instruments at both levels are exposed at heights greater than $2z_H$, both instrument levels yield representative local-scale flux measurements. However, when the tower is in the D position, only the upper measurement level provides local-scale fluxes. In this dense urban setting, these results provide further support of the guideline of about $2z_H$ as the minimum height required to obtain representative local-scale fluxes at a densely

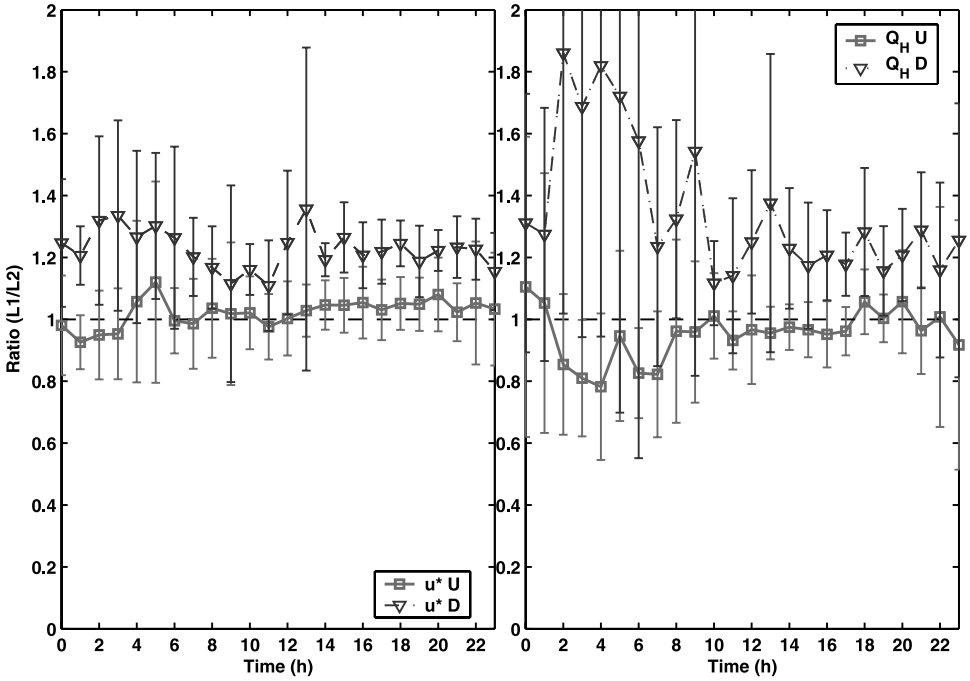

Figure 3. Mean and standard deviation of the ratio by level of u* and Q_H (L1/L2) when the tower is in the U and D positions by time of day. See color version of this figure in the HTML.

developed site and gives confidence that such fluxes are being analyzed here.

3.3. Albedo and Radiation Fluxes

[20] The surface albedo was determined from the observations at the two heights when both the incoming and outgoing solar radiation were >5 W m^{-2}. The diurnal "U"-shaped pattern (Figure 4) is remarkably similar to that observed over less rough surfaces such as low plant covers, bare soil, snow, ice and water bodies [*Oke*, 1987]. This pattern has been seen in other urban studies [*Rouse et al.*, 1973; *White et al.*, 1978; *Offerle et al.*, 2003]. In the middle

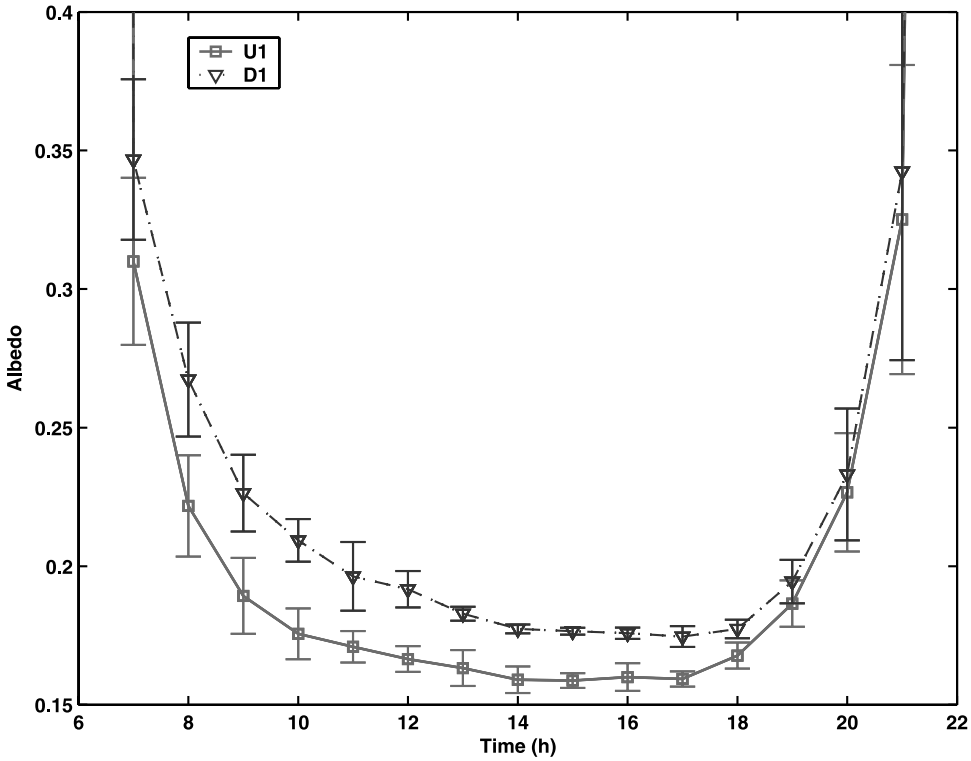

Figure 4. Mean and standard deviation of surface albedo with height (U1, D1). See color version of this figure in the HTML.

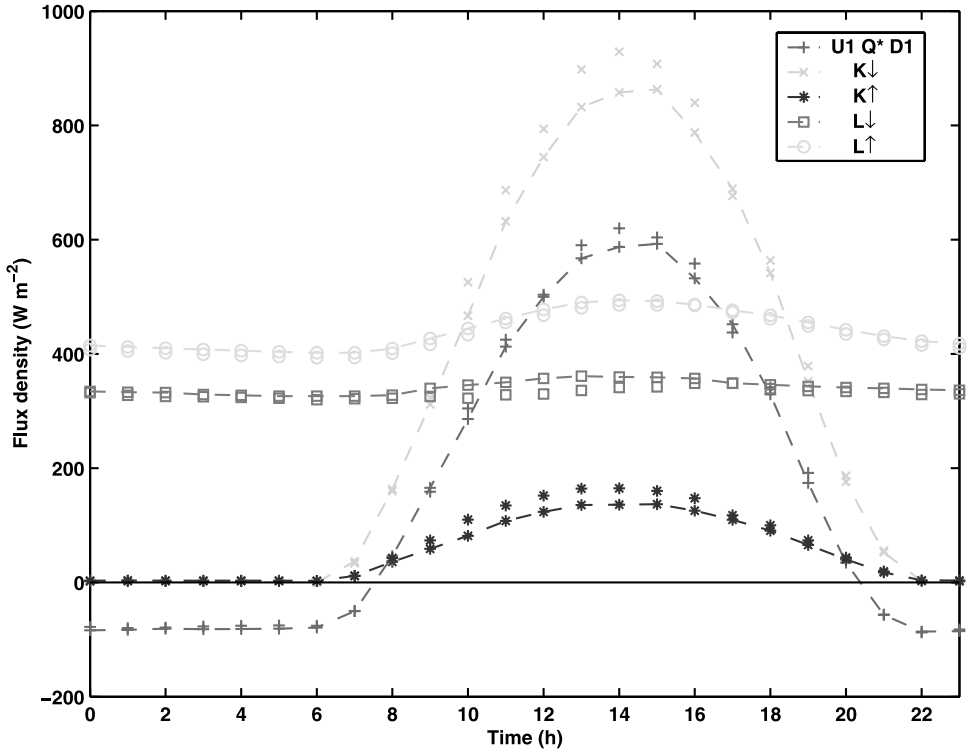

Figure 5. Mean radiation balance at the U1 (lines with symbols) and D1 (symbols) levels. See color version of this figure in the HTML.

of the day, the albedo is 0.16 when the tower is at the U1 level, and 0.18 when the tower is more retracted (D1) (Table 1). As *Reifsnyder* [1967] described, and *Offerle et al.* [2003] and *Soux et al.* [2004] demonstrate, the height of a radiation sensor influences the number of microscale units (building and canyons) the sensor "sees," and thus the representativeness of the observations. It also affects the proportions of facet types seen (i.e., roofs, walls and road [*Soux et al.*, 2004]). At this site, the albedo determined from the U1 level should yield the most representative local-scale value for the city center area. In particular, it probably gives a better representation of facet types is relevant because the roof of the CAA building is covered with light-colored gravel (albedo ~0.21 [*Roberts et al.*, 2003]) and it has a larger influence on the tower-observed albedo the lower the down-facing pyranometer is mounted.

[21] The asymmetry in the diurnal course of albedo (Figure 4) suggests that either the sensor is not exactly level or that surface and/or meteorological factors influence the radiation exchanges differently in the morning and afternoon. The varying sun/shade patterns and the associated changes in the role of particularly high- or low-albedo surfaces through the day can result in temporal asymmetry of the upwelling flux. Further, this site has deep urban canyons, thus shadows and canyon orientation affect albedo. The effect of canyon geometry (specifically the height to width ratio) on albedo is well documented [*Aida*, 1982; *Arnfield*, 1982], however, previous modeling studies only consider symmetrical canyons [*Aida*, 1982; *Arnfield*, 1982; *Pawlak and Fortuniak*, 2003]. At the CAA site, the urban configuration is complex and asymmetric. Although the pyranometer's field of view (FOV), and thus albedo, does not vary with wind direction, differences in air quality, haziness, and cloud may change with winds from different directions are another potential source of asymmetry. For example, at times when the mast was fully extended, U1, and the wind was from directions 120°–180°, clouds tended to be present in the early afternoon (1300–1400 LT), with an associated reduction in K↓, K↑ and Q*.

[22] Given these characteristics it is not surprising that the diurnal course of albedo (Figure 4) is asymmetric. The difference through the course of the day (1000–1700 LT) when measuring at one height is about the same size, 0.02, as the difference observed between measurements at the two heights (U1 and D1). The diurnal asymmetry of albedo is greater from the lower measurements, D1 (0.028 compared to 0.016 at U1), which is consistent with shadows being a more significant part of the FOV when the tower is retracted.

[23] The incoming and outgoing shortwave and longwave radiation fluxes are categorized into two periods: when the tower was retracted (D) typically during mistral wind conditions; and when it was more fully extended (U), sea breeze and all other wind conditions. Generally, clearer skies were associated with times of the mistral wind, resulting in slightly greater solar radiation in the morning hours when the tower was down (D) (Figure 5). The outgoing longwave radiation is essentially the same regardless of tower height or wind. The morning incoming longwave radiation is slightly less for D1 than U1, as is to be expected because of the clearer and cooler skies during mistral conditions. Overall, the mean net all-wave radiation is very similar for the two sets of conditions (U and D) with

Table 5. Mean Energy Balance Fluxes Measured at L1 for the Study Period, by Prevailing Wind Régime and by Tower Location[a]

	Condition 1									Condition 2				
	Q*	Q_H	Q_E	ΔQ_S	Q_H/Q^*	Q_E/Q^*	$\Delta Q_s/Q^*$	β	N	Q*	Q_H	Q_E	ΔQ_S	N
24 Hours														
All	163	154	38	3	0.95	0.23	0.02	4.02	25	164	153	39	5	19
Other	157	152	31	6	0.97	0.20	0.04	4.85	6	159	153	31	7	5
Mistral	173	164	50	−9	0.95	0.29	−0.05	3.28	4	173	164	48	−7	4
Sea breeze	162	152	38	6	0.93	0.23	0.03	4.01	15	163	149	39	8	10
Q > 0 (13 Hours)*														
All	364	253	61	98	0.69	0.17	0.27	4.17	25	367	252	59	104	19
Other	350	248	50	98	0.71	0.14	0.28	4.95	6	353	249	47	104	5
Mistral	386	269	73	91	0.70	0.19	0.24	3.66	4	386	269	69	95	4
Sea breeze	365	251	61	100	0.69	0.17	0.27	4.08	15	366	246	60	108	10
24 Hours														
D1	170	172	41	−11	1.01	0.24	−0.06	4.18	7	170	172	42	−12	7
U1	165	148	42	7	0.90	0.26	0.04	3.49	9	167	145	40	15	6
U1↔D1[b]	155	145	32	10	0.94	0.20	0.07	4.58	9	155	140	35	13	6

[a]Mean energy balance fluxes are given in W m^{-2}. See Figures 2 and 6 for prevailing wind régimes. Condition 1 consists of the averages of all data, whereas for condition 2, spikes in the latent heat flux have been removed (see text for more details). N is the number of complete days. Q_F is estimated to be 33 W m^{-2}.

[b]U1↔D1 refers to days when the tower was moved between positions.

the greatest difference (<50 W m^{-2} in the average) just before solar noon.

3.4. Energy Balance Fluxes

[24] In this study, the terms not directly observed in the surface energy balance are the anthropogenic heat flux, advection, and storage heat flux. The anthropogenic heat flux (Q_F) is a function of the number of vehicles driven within the area, the energy used within buildings, and the energy released as part of metabolism [*Grimmond*, 1992; *Sailor and Lu*, 2004]. Unfortunately, such data are not available for the study site in Marseille. However, *Sailor and Lu* [2004] recently made estimates of the temporal variation of Q_F for several large U.S. cities, and *Ichinose et al.* [1999] do the same for central Tokyo, Japan; *Harrison et al.* [1984] and *Kłysik* [1996] include both temporal and spatial variations for the densely built cities of London, UK, and Łódź, Poland, respectively. On the basis of these and other published analyses the diurnal pattern of Q_F for central Marseille was assigned as follows: nighttime value of 15 W m^{-2}, daytime value of 50 W m^{-2}; with an hour transition, to a morning and late afternoon peak value of 75 W m^{-2}. The timing of these peak values are based on the F_{CO2} results (section 3.7), which provide an independent measure of human activity near the Marseille site. As previous discussions indicate, the observed surface energy balance already incorporates some of the anthropogenic heat flux. For example, the net all-wave radiation is reduced because of increased surface temperature [*Grimmond*, 1992; *Crawford and Grimmond*, 2003]. The turbulent sensible heat flux measured above the canopy also includes emissions of heat from vehicles. However, because the storage heat flux term is derived as a residual, i.e., it is not directly measured, any anthropogenic heat that causes the urban soil-building-air volume to heat up needs to be included.

[25] The horizontal advective terms for this measurement period are difficult to determine with our observations. *Pigeon et al.* [2003] used their network of temperature and humidity sensors, located at approximately the top of the urban canopy layer in Marseille, and a mesoscale model to determine these fluxes for 1400 local time (LT) on 4 days in the ESCOMPTE campaign. Their results indicate that the moisture and heat flux advection are of similar size but of opposite sign. They conclude that they cancel each other out.

[26] Here, the storage heat flux is determined as a residual from the observations, including an estimate of Q_F but not the advective terms. Therefore the storage heat flux accumulates the errors due to measurement uncertainty and the unmeasured terms [*Grimmond and Oke*, 1999b]. In forested sites, where energy balance closure has received significant attention in recent years, it has been noted that in most cases, closure of the energy balance is not obtained from observations [*Wilson et al.*, 2002; *Oliphant et al.*, 2004]. Moreover, it appears that the turbulent heat fluxes may be under observed. The results presented here should be considered with these caveats in mind.

[27] Controls on surface energy balance fluxes are complex and relate to both atmospheric and surface influences. Given the different atmospheric and fetch (surface) conditions related to the mistral and sea breeze wind régimes, here we consider the surface energy balance fluxes for the entire study period and then discuss differences under the influence of the sea breeze (U) and mistral (D) conditions.

[28] The overall energy balance fluxes for the entire study period are summarized in Table 5. The fluxes presented come from those days with complete data for the 24 hours or for the daytime period. If a 1 hour gap occurred, missing data were filled in by linear interpolation of data from the surrounding hours. On the basis of hour-by-hour inspection of the fluxes, it is apparent that for individual hours the moisture signal produces large excursions of Q_E. For this reason, the initial or first averages were computed when all data were considered (for the conditions listed above), referred to hereafter as condition 1 (C1). A second set of averages was calculated with the hours having large excursions removed (referred to hereafter as condition 2 (C2)) (Q_E fluxes removed when $\sigma_q > 0.2$ g m^{-3} when $Q_E > 200$ or <-35 W m^{-2}). The day-to-day variability of the average daily fluxes for both sets of conditions is presented in

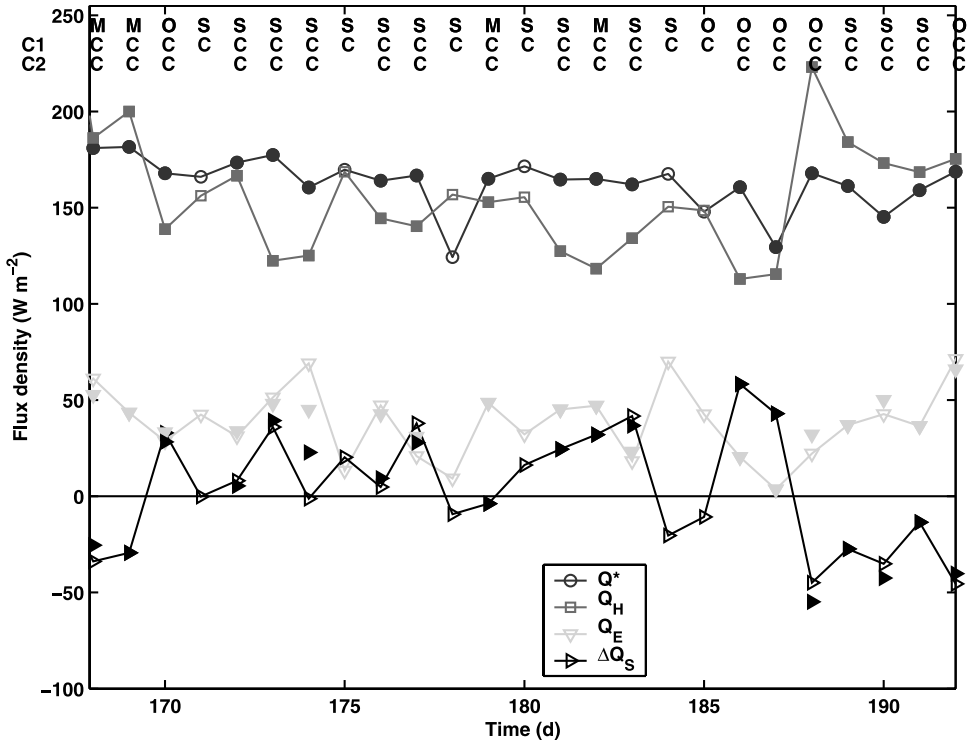

Figure 6. Mean daily fluxes for each day of the observation period. The upper line of text gives information on the prevailing wind régime (M, mistral; S, sea breeze; O, other). On the next two lines, C indicates complete 24 hour data coverage with the presence of data for condition 1 on line C1 (see Table 5 and text) and with the presence of data for condition 2 on line C2. The data connected with lines and open symbols are for condition 1; the solid symbols are for condition 2. See color version of this figure in the HTML.

Figure 6 (open symbols indicate C1, and closed symbols indicate C2).

[29] Clearly, for Marseille, Q_H accounts for the largest fraction of energy, with an overall fraction of 0.95 of Q*. However, for individual days the ratio varies widely, from 0.69 to 1.32. Under sea breeze conditions Q_H/Q^* is slightly smaller, on average (0.93). The storage heat flux (ΔQ_S) peaks before solar noon and turns negative one or two hours before Q* (Figure 7). Prior to the solar peak the partitioning of the sensible heat between convection and conduction is almost equal; but in the afternoon convection dominates, with a peak in the early afternoon. The phase shift of Q_H relative to Q* is substantial in the later afternoon, and in the evening Q_H remains directed away from the surface. This is a known feature of heavily developed urban sites (see *Grimmond and Oke* [2002] for a more full discussion). There is a large loss of heat storage through the nighttime period, indeed the $\Delta Q_S/Q^*$ ratio is considerably greater than 1 (Figure 8). The heat storage régime at this site is considered in more detail by *Roberts et al.* [2003]. The role of changing conditions through the study period is also evident in ΔQ_S. The net storage heat flux is expected to tend to zero over longer time periods, with excursions of net gain and loss based on synoptic conditions. For the overall study period, ΔQ_S averages 3 W m^{-2} (condition 1), but if spikes in Q_E are removed (condition 2), it averages 5 W m^{-2} (Table 5). It should be noted, however, that the net ΔQ_S is influenced by the size and timing of the assumed Q_F term. For example, if our estimated daytime Q_F were reduced to 40 W m^{-2} it would give a net ΔQ_S of 0 and 1 W m^{-2}, for conditions 1 and 2, respectively. The time periods of greatest net heat loss from the urban fabric are, as expected, during mistral wind conditions.

[30] The latent heat fluxes (Q_E) measured at the CAA site generally are small, as expected given the relatively small fractions of vegetation cover and open water in the source area of the turbulent flux measurements, and the lack of precipitation in the study period. However, the latent heat fluxes are not negligible ($Q_E/Q^* = 0.23$) and are larger than those observed in Mexico City (Me93) and at a light industrial site in Vancouver (Vl92) [*Grimmond and Oke*, 2002]. The combined plan area fraction of vegetation and water is much greater in Marseille (10–20%) than in Me93 and Vl92 where it was $\ll$10% (see section 3.6). Also, street cleaning, using water from the city main water pipes, appears to be more common in Marseille than in Me93. The daytime Bowen ratio (Q_H/Q_E) fluctuates around 3–4. At night small latent heat fluxes (<20 W m^{-2}) continue. Variations in moisture associated with differences in wind directions are also important on an hour-to-hour and day-to-day basis. This issue is considered further in section 3.5. Under mistral wind conditions the Q_E/Q^* ratio is greatest.

[31] It should be noted that all of the fluxes have a larger absolute magnitude, on average, under mistral conditions. This is partly due to the clearer air and therefore increased Q*. When the tower was in the U1 (sea breeze typically) and D1 (mistral typically) modes, observed differences in the turbulent sensible heat flux are greater than differences

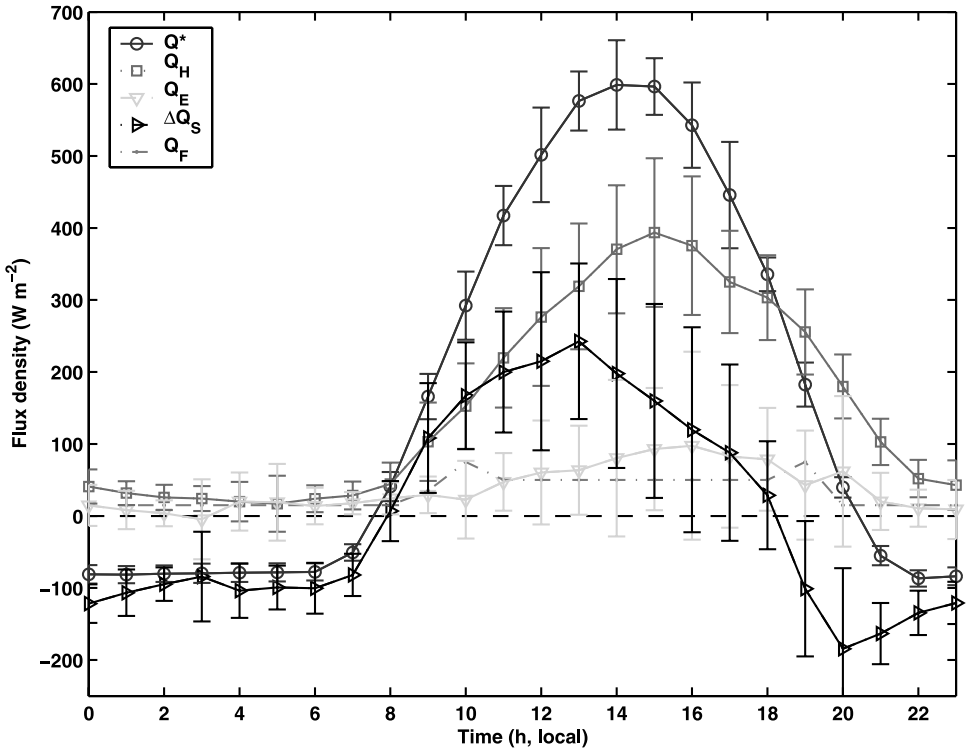

Figure 7. Mean and standard deviation of the energy balance fluxes for all L1 (U1 and D1) data for the study period for condition 1 of Figure 6. See color version of this figure in the HTML.

in the forcing radiation flux (Table 5). Observations from the D1 position show Q_H values that are slightly greater than Q* on average.

[32] The mean diurnal pattern of the energy balance fluxes for the observation period, with standard deviations, is shown in Figure 7. It is useful to consider the variability between individual observation periods to determine the consistency of the mean results. The variability can be compared to the data stratified by wind régimes in Figure 8. Only on rare occasions is the nocturnal Q_H negative, although there is variability from day to day of the order of 100 W m^{-2}. As expected, the daytime variability is greater.

[33] The turbulent source area characteristics change with both meteorology and the height of the instrumentation. The roofs and impervious surfaces are always the predominant fractions of the source area (Figure 8) but the role of the water in the old port changes with wind conditions (see Figure 10 of *Lemonsu et al.* [2004a]). Under mistral conditions the water fraction is larger than the vegetation fraction (Figure 8). The ''other'' days are characterized as being the least influenced by the presence of the port. It should be noted that the radiative source areas also change with the tower position. However, the U1 and D1 L↑ values (Figure 5) are similar despite the FOV changes of the radiometer. The temperature close to the surface (from temperature profile measurements) is cooler in all periods under mistral conditions compared with other days and the temperature profile gradient is also much smaller (see also section 3.8).

[34] Comparison of the flux partitioning according to wind régimes shows, that during morning hours the partitioning between turbulent and conductive sensible heat differs. Under mistral conditions Q_H is larger than ΔQ_S, whereas for the other two régimes their size is more similar. The $\Delta Q_S/Q^*$ and Q_E/Q^* ratios show the reverse relative ordering by wind régime, with the mistral conditions having the larger Q_E/Q^* fraction. Bowen ratio ($\beta = Q_H/Q_E$) values are similar, but because Q_E is small relative to Q_H there is a lot of variability on an hour-to-hour basis between wind régimes (Figure 8). On a diurnal basis, under mistral conditions the greatest difference is in the increased Q_E/Q^* which results in a smaller β. This is in agreement with the increased presence of water in the source area, which unlike the vegetation has no restriction on evaporation. The reduced daytime $\Delta Q_S/Q^*$ and the continued large Q_H and Q_E during the night result in the net loss of ΔQ_S under mistral conditions.

3.5. Short-Term Variability in Water and Carbon Dioxide

[35] Sources and sinks of water and carbon dioxide in urban environments are always patchy. In Marseille this is particularly true: the sparse vegetation (Figure 1), which is a source of water and a sink of carbon dioxide, largely exists in courtyards except for one boulevard, and the primary source of carbon dioxide is traffic, which is largely restricted to the network of streets. In previous studies of the latent heat flux in cities using eddy covariance techniques, the fluxes have been noted to be variable over short periods [*Grimmond and Oke*, 1995; *Grimmond and Oke*, 2002].

[36] When the Marseille data are viewed in detail, sudden short-term excursions both positive and negative in the signal, away from and toward the surface, respectively, occur in both water vapor and carbon dioxide fluxes at a

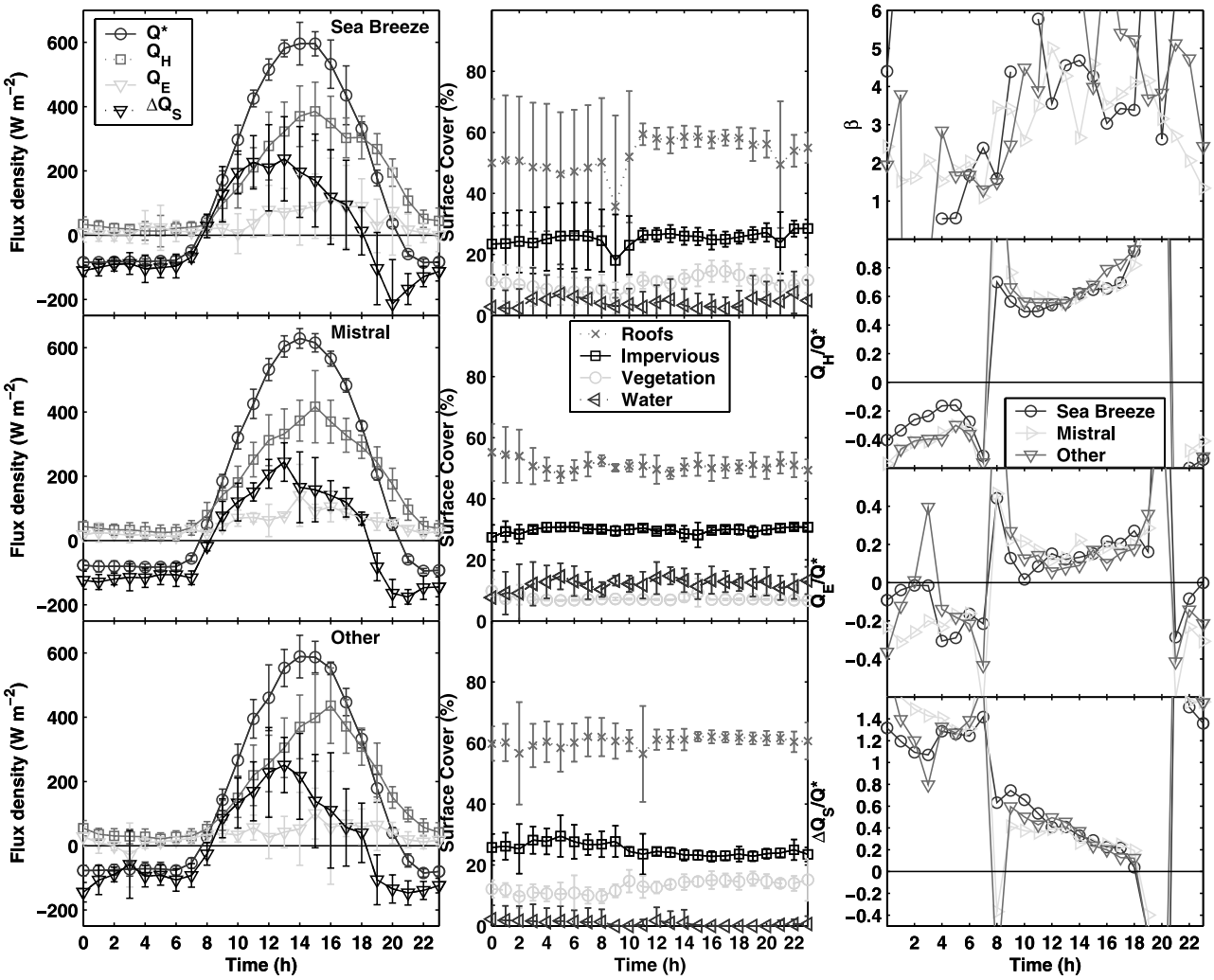

Figure 8. Mean and standard deviations of the surface energy balance fluxes (left column) for days defined as sea breeze (top), mistral (middle), and other (bottom). Mean and standard deviation of surface cover characteristics in the flux source area associated with these conditions (middle column). Normalized fluxes compared by wind condition (right column) for Bowen ratio (Q_H/Q_E) (top panel) and turbulent sensible heat flux (Q_H/Q^*), latent heat flux (Q_E/Q^*), and net storage heat flux ($\Delta Q_S/Q^*$) (bottom three panels). See Figure 6 for definitions of days. See color version of this figure in the HTML.

variety of timescales (5, 10, 15, 30 and 60 min averaging times) throughout the data set. These excursions occur in data from both levels, with some coincidence in the timing at different heights and in more than one scalar variable. In many instances the anomalies in fluxes evident at longer time periods are traceable back to such excursions at the 5-min scale; therefore the 5-min fluxes were analyzed in more detail. In order to isolate these values objectively from the data set, cutoff values of ±250 W m^{-2} were chosen for water vapor fluxes and ±50 μmol m^{-2} s^{-1} for carbon dioxide fluxes. Spikes due to sensor malfunction are excluded.

[37] The excursions frequently coincide with marked jumps in mean concentration of the scalar, suggesting that they may be an inadvertent product of the Reynolds averaging process rather than being a true peak in the flux. To test this hypothesis, jumps in concentration were identified on the basis of cutoff values of 0.5 g m^{-3} for water vapor and 0.25 mmol m^{-3} for carbon dioxide (Table 6). Although there were more excursions in water vapor concentration than in water vapor flux, more than 90% of the flux spikes can be attributed to this phenomenon. More than 70% of the excursions in the carbon dioxide flux (F_{CO2}) coincided with jumps in mean carbon dioxide concentration.

[38] These findings suggest that the nonstationarity associated with abrupt discontinuities in the air mass characteristics at the site may be a significant causal factor in the incidence of spikes in the respective fluxes. As noted

Table 6. Total Number of Excursions in the 60 min Mean Concentration Data by Level by Wind Régime

	Number of 60 min Periods With Excursions					
	H_2O Concentrations			CO_2 Concentrations		
	Other	Mistral	Sea Breeze	Other	Mistral	Sea Breeze
L1	30	7	106	11	1	80
L2	34	7	127	7	3	69

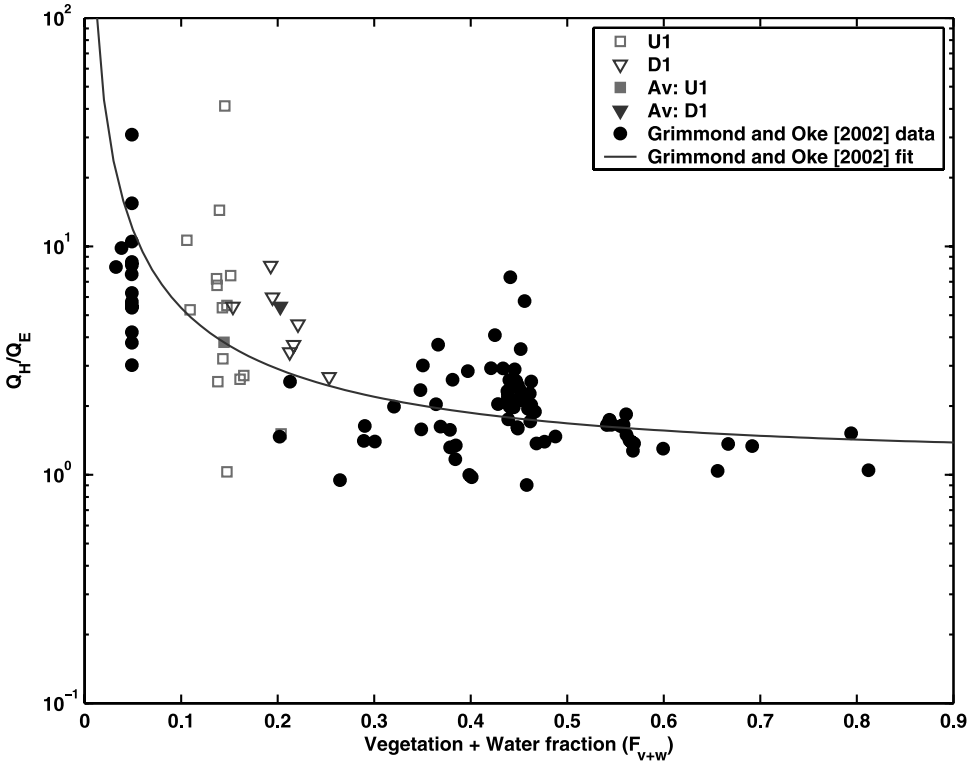

Figure 9. Bowen ratio versus vegetation plus water fraction for midday period. The line and solid black circles are data from *Grimmond and Oke* [2002] (see their Figure 5b). The open symbols are the individual days, and the solid symbols are the average for the observations. See color version of this figure in the HTML.

earlier, winds at this site were highly polarized along the SE-NW axis during the observation period, with mistral flow dominating NW flows. Given the coastal location of Marseille we might expect to see quite different air mass characteristics with wind direction.

[39] Our results indicate that for water vapor there is an increased probability for jumps in concentration when winds are from the SW and NE sectors. The corresponding weighted distribution of carbon dioxide jumps shows that spikes occur most with flow from the N and NNE sectors. These are ratios of small numbers in most instances. The main NW-SE wind direction axis is almost free of excursions. This may be attributable to the spatial and temporal consistency of the mistral wind and the enhanced mixing from this direction.

3.6. Variability of Turbulent Fluxes With Surface Cover

[40] The influence of surface properties on the turbulent heat flux partitioning can be evaluated using the *Schmid* [1994] 2-D FSAM source area model to determine source area properties influencing the flux observations at any given time (see section 2.2.2). One index of surface cover shown to be to be related to flux partitioning, specifically the Bowen ratio, is the fraction of the surface irrigated [see *Grimmond and Oke*, 2002]. Figure 9 shows the Bowen ratio and the corresponding mean vegetation fraction using data from the 4-hour period centered on solar noon. The midday mean Bowen ratio of 5.5 (D1) is associated with source areas that are on average 11% vegetated (+9% water). For U1 the mean midday Bowen ratio is 3.8 associated with 14% vegetation (<1% water). The Marseille data conveniently occupy a gap in the relation and show similar variability from day-to-day to that at other sites. The average value (solid symbol) for the data for each level are close to what is predicted on the basis of *Grimmond and Oke* [2002]. This suggests that the LUMPS approach to parameterizing the turbulent heat flux partitioning is probably valid in this high-density urban area.

3.7. Carbon Dioxide Fluxes

[41] In comparison to other environments, in particular forests [*Baldocchi et al.*, 2001], there are relatively few observations of carbon dioxide fluxes (F_{CO2}) from urban sites. Those published include data for a suburban/commercial area of Chicago [*Grimmond et al.*, 2002a], the city core of Edinburgh [*Nemitz et al.*, 2002], and residential areas of Copenhagen [*Soegaard and Moller-Jensen*, 2003], Tokyo [*Moriwaki and Kanda*, 2004], and Basel [*Vogt et al.*, 2004]. In most of these cases, as with Marseille, the sites are in areas with little vegetation and heavy traffic.

[42] The observed F_{CO2} for Marseille indicates that the central area of the city acts as a source of CO_2 (Figure 10). Since these measurements were taken close to the peak of the growing season, they suggest that the central city core will be a source of carbon dioxide throughout the year. The diurnal pattern of F_{CO2} reveals the impact of the daily traffic cycle on emissions. In the midafternoon, 1400–1600 LT, F_{CO2} is reduced, probably because of a reduction in traffic, and small uptake by vegetation (Figure 10), then increases

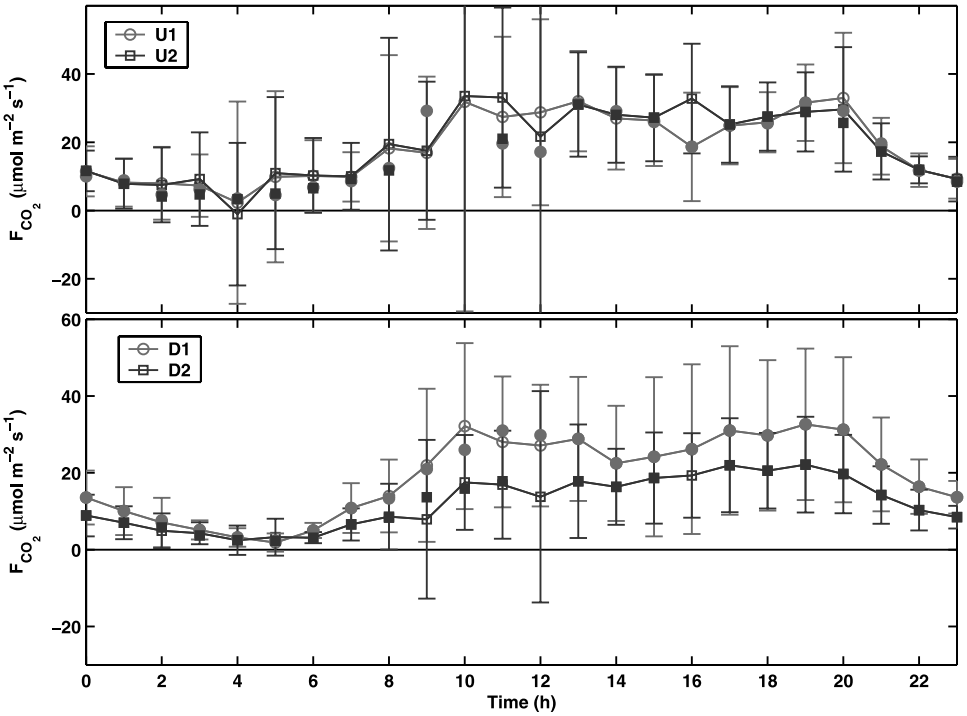

Figure 10. Mean diurnal pattern of F_{CO2} by level for the observation period (open symbols) with standard deviations. Solid symbols mean for periods when $\sigma_{CO2} < 0.2$ mmol m^{-3}. In both cases, N had to be greater than 5 for an individual hour to be plotted. See color version of this figure in the HTML.

again between 1700 and 2000 LT. The morning peak is larger than the afternoon peak. In the period between 0400 and 0600 LT there is almost a zero flux. This is a time when human activities are at a minimum and given the relatively small area of vegetation in the source area plant respiration is also low.

[43] The magnitude of the average F_{CO2} and the diurnal pattern reported in this study are comparable to those reported from the other studies of central urban sites (in Edinburgh, mean values of 22 μmol m^{-2} s^{-1} are reported, and in Basel, values typically range from 10 to 20 μmol m^{-2} s^{-1}, with peak values of 30 μmol m^{-2} s^{-1}) and approximately twice the magnitude of the average values reported in a more residential, heavily treed neighborhood of Chicago [*Grimmond et al.*, 2002b]. In all the cities peak values, as in Marseille, are associated with rush hour traffic.

[44] Like the case of Q_H, the average fluxes are very similar when the tower is extended (U1, U2), except for periods when σ_{CO2} is very large. The solid data symbols in Figure 10 are the mean when $\sigma_{CO2} < 0.2$ mmol m^{-3}. Some of the apparent dips in the diurnal cycle, especially for the U data, are caused by a few large departures from the mean. When the tower is in the D position there is greater difference between the two levels. This highlights, again, the importance of the measurement height in local-scale flux comparisons.

3.8. Stability Conditions

[45] Given the relatively small number of observational studies of turbulence in urban areas, and the importance of this information to predicting dispersion behavior and selecting appropriate coefficients (for example, for wind profile related functions), it is important to know the mean stability conditions in an urban environment such as Marseille, plus the variability of stability and probability of these conditions occurring. It is common practice in air pollution dispersion calculations to assume that urban atmospheres tend to remain unstable or neutral at night, rather than becoming stable as in the rural case. Direct evidence of this fact is sparse however, prompting calls by the dispersion and diffusion communities to document these stability properties [*Dabberdt et al.*, 2004].

[46] The Obukhov stability length (L) was calculated for each measurement level for each time period. Overall, less than 1% of the data at each level were stable ($z'/L \geq 0.1$). The conditions are frequently (85%) unstable ($z'/L < -0.1$) at levels U1 and U2. At the D1 and D2 levels, >60% of the data are close to neutral $|z'/L \leq 0.1|$ otherwise conditions are unstable. In comparison, <15% are close to neutral $|z'/L \leq 0.1|$ for the U1 and U2. The mean generally indicates more unstable conditions than the median (50th percentile) (Figure 11). On the basis of air temperature profile data on the CAA mast, the temperature gradient is close to neutral throughout the nocturnal period under mistral conditions. On the other hand, for the remaining days it remains unstable until ~0400 LT and then becomes slightly stable until ~0700 LT. The results are similar between levels (U1 and U2 versus D1 and D2), which suggests the importance of studying a wide range of meteorological conditions in urban settings. Because of lower wind speeds the surface layer is often more unstable at night than in the daytime. Similar results between measurement levels suggest that this

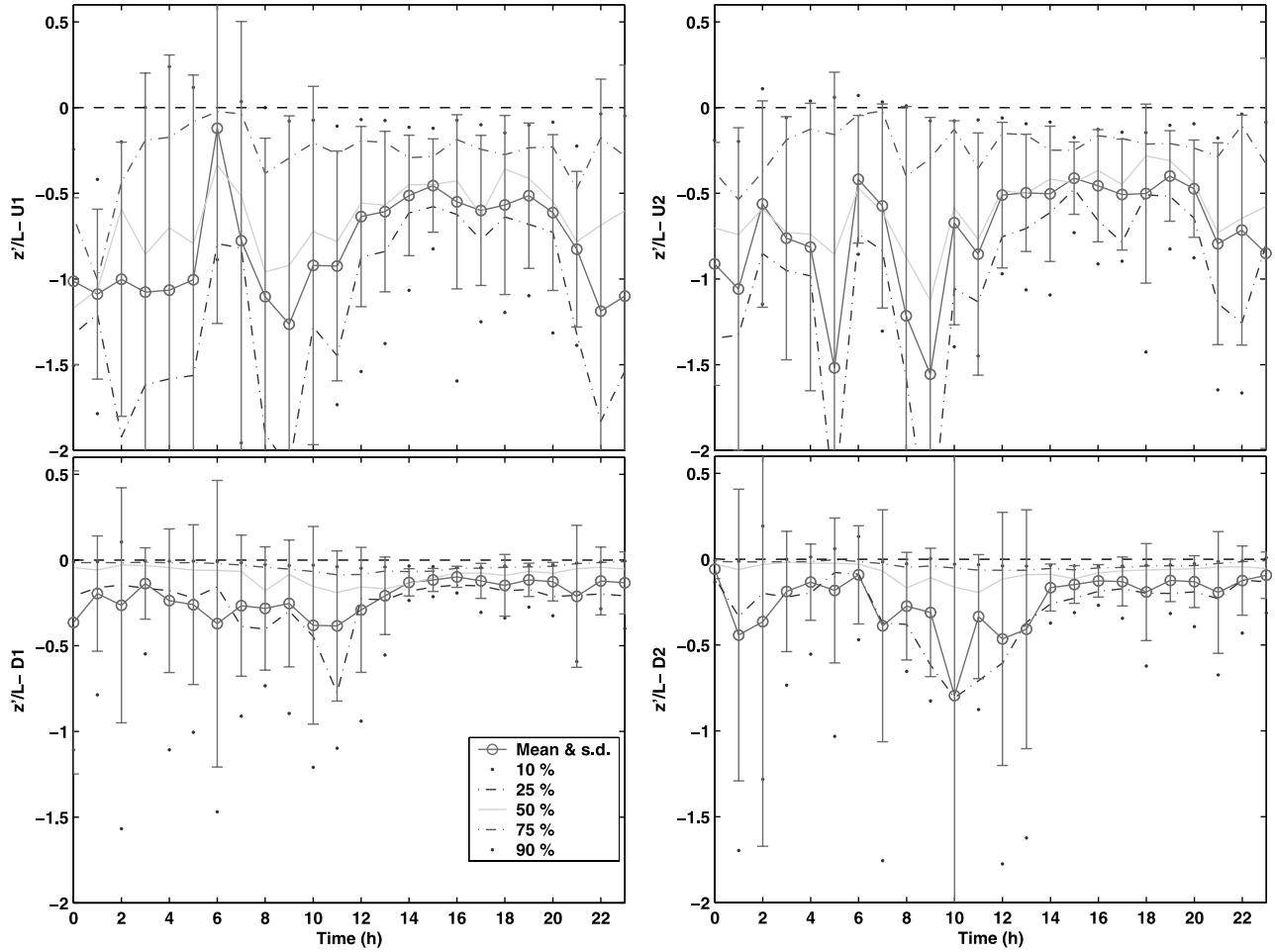

Figure 11. Diurnal pattern of stability by level (U1, U2, D1, and D2). Mean, standard deviation, and 10th, 25th, 50th, 75th, and 90th percentiles are shown. See color version of this figure in the HTML.

is spatially well averaged and consistent with the release of heat stored in the urban fabric

3.9. Variability of Turbulence Characteristics

[47] *Roth* [2000] provided a comprehensive historical review of the atmospheric turbulence data collected in urban areas. He notes the relatively small amount of data available for his synthesis. There is need to expand the data available to test the universality of both theoretical and empirical relations. *Roth* [2000] reworked the original data into a common framework and used it to develop statistical relations. Here we compare Roth's relations with the data collected in Marseille. The data from all four levels are used. As with *Roth* [2000] the synthesis involves a series of normalizations wherein the height of measurement is expressed relative to the size of the roughness elements. By collapsing the height scale, comparison with other urban sites becomes possible (see section 2 for notation definitions). Here neutral conditions are defined as $|z'/L| \leq 0.1$.

[48] In many circumstances the drag coefficient ($C_D^{0.5}$ = u*/U, where u* is friction velocity and U is the mean wind speed) is used instead of the roughness length for momentum to describe the role of surface roughness on the turbulence and wind fields. In Marseille under neutral conditions the data fall close to the line that expresses the log law wind profile (Figure 12). In this plot the mean

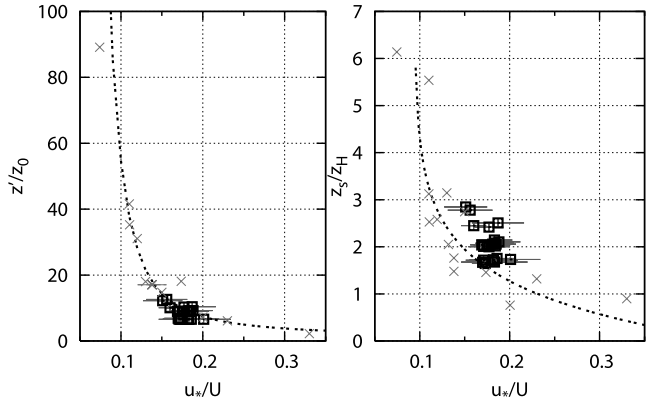

Figure 12. Variation of u*/U for neutral conditions with nondimensional heights (left) z'/z_0 and (right) z_s/z_H. Mean and standard deviation are shown for a normalized height and direction data. Line in left panel is based on log profile, and line in right panel is based on *Roth* [2000, equation (5)] ($u^*/U = 0.094 + 0.353 \exp[-0.946(z_s/z_H)]$). Squares are data from this study, and crosses are data reported by *Roth* [2000, Figure 1]. See color version of this figure in the HTML.

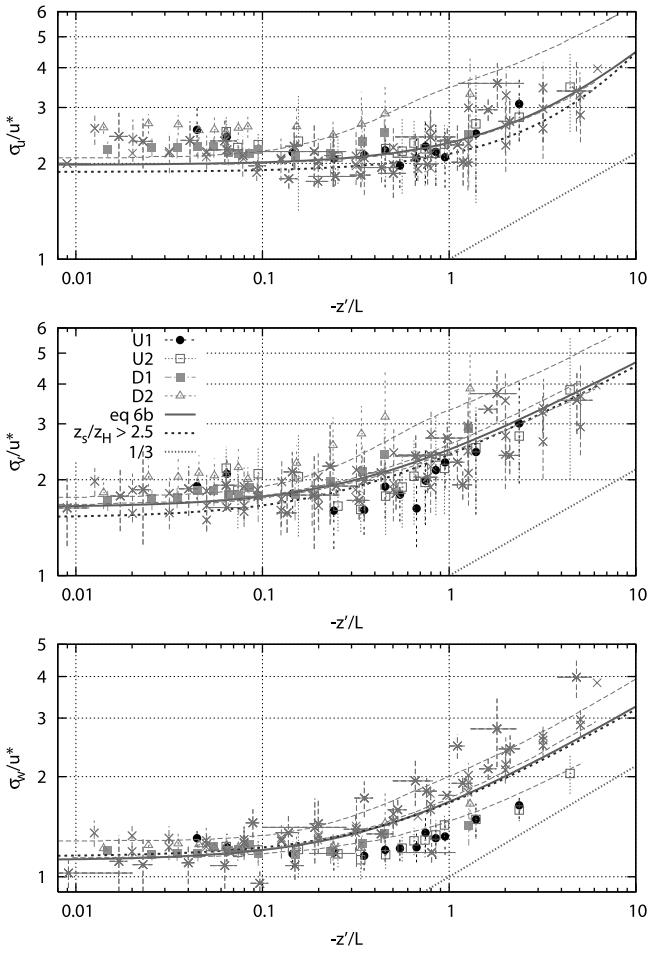

Figure 13. Variation of (top) $A_u = \sigma_u/u^*$, (middle) $A_v = \sigma_v/u^*$, and (bottom) $A_w = \sigma_w/u^*$ with unstable stability (logarithmic scale) with *Roth* [2000, Figure 4] data. Mean and standard deviation are shown for each level binned by stability. Dotted, blue lines and solid, red lines are from *Roth* [2000, equation (6b)] using his Table 5 $z_s/z_H > 2.5$ and all coefficients, respectively. The 1/3 slope is also shown. See color version of this figure in the HTML.

roughness length to one significant figure is used rather than a fit to the log law for the individual directions. This result is similar to that found at Sapporo (S92) (see Figure 1 of *Roth* [2000]). The data fall to the right of the line predicted by *Roth* [2000]. Given the other results lie to the left of the line it suggests that his equation (5) is applicable to this type of dense urban core for determination of the drag coefficient (Figure 12).

[49] In many dispersion applications it is necessary to specify the standard deviations of the wind velocities (σ_i). The normalized velocity standard deviations ($A_i = \sigma_i/u^*$ where i = u, v, w) for longitudinal (u), lateral (v) and vertical (w) wind velocities were determined for neutral conditions. The A_u value are scattered around 2.40; A_v shows the greatest variability and is centered around 1.93, whereas A_w is the least variable with an overall mean of 1.22. In all cases, these are slightly less than the mean values suggested by *Roth* [2000] for $z_s/z_H < 2.5$, but are within the limits suggested by *Panofsky and Dutton* [1984]. Figure 13 shows the variation of A_i with increasing instability. The best fit using the empirical relation of *Roth* [2000, equation (6b)] is for the more unstable portion of A_u. With increasing instability each set of Marseille data approaches the 1/3 slope predicted by Monin-Obukhov similarity. The D2 data, which show the greatest scatter, are still similar to that given by *Roth* [2000, Figure 4] when using smaller z_s/z_H data sets.

[50] Figure 14 shows the turbulence intensities ($I_i = \sigma_i/U$ where i = u, v, w) for neutral conditions. The lines are based on theory [*Roth*, 2000, equation (8)]

$$\sigma_i/U = kA_i[\ln(z'/z_0)]^{-1}$$

and Roth's empirical fit to the available data (his equation (9)) (right). Both lines are generally good descriptions of the Marseille data, with the I_u data having the least scatter. When turbulent intensities, I_i, are plotted relative to stability, Roth found considerable scatter, with almost all of the data falling above the Monin-Obukhov similarity predictions. In Marseille this pattern is also evident (Figure 15) with the data following a trend of increasing I_i with increasing instability. In Marseille, there were not enough stable conditions to provide data points in that stability régime.

[51] The Marseille data have larger I_i values than the V89 and S76 data plotted by *Roth* [2000]. Probably this is to be expected given the larger roughness in Marseille compared to the Vancouver and St Louis sites. The Zurich data (Z86) used by Roth, which is more similar in roughness characteristics to Marseille, had more comparable values, but the Z86 data are for a more restricted range of stability conditions.

4. Conclusions

[52] These data from the city core of Marseille help to fill a gap in our understanding of surface energy balance fluxes and turbulence data in cities. The combination of wind and surface properties creates an interesting range of conditions in which to conduct observations. It is clear from the analysis that care is needed when stratifying and averaging data from such sites. Here the height of measurement, wind direction, and the surface character associated with these observations were all considered. The surface energy balance partitioning is largely as expected, with large turbulent sensible heat fluxes dominating the daytime. Under the three different wind régimes considered here the fluxes vary most in the morning. The small amount of vegetation present plays a more influential role after solar noon by generating small but significant latent heat fluxes and reduced carbon dioxide fluxes. Mistral winds act to reduce concentrations of pollutants in the urban atmosphere, which in turn results in increased net all-wave radiation and increased sensible heat flux. The Bowen ratio for this site falls close to that predicted by the *Grimmond and Oke* [2002] relation on the basis of the fraction of the surface covered by vegetation.

[53] The Marseille data provide much needed information on the stability conditions in central city environments. They also allow comparison with the synthesis of turbulence data for urban areas forwarded by *Roth* [2000]. In general, the Marseille data provide support for the empirical functions proposed by Roth. In cases, such as the relation of turbulence intensity with stability, where there are few

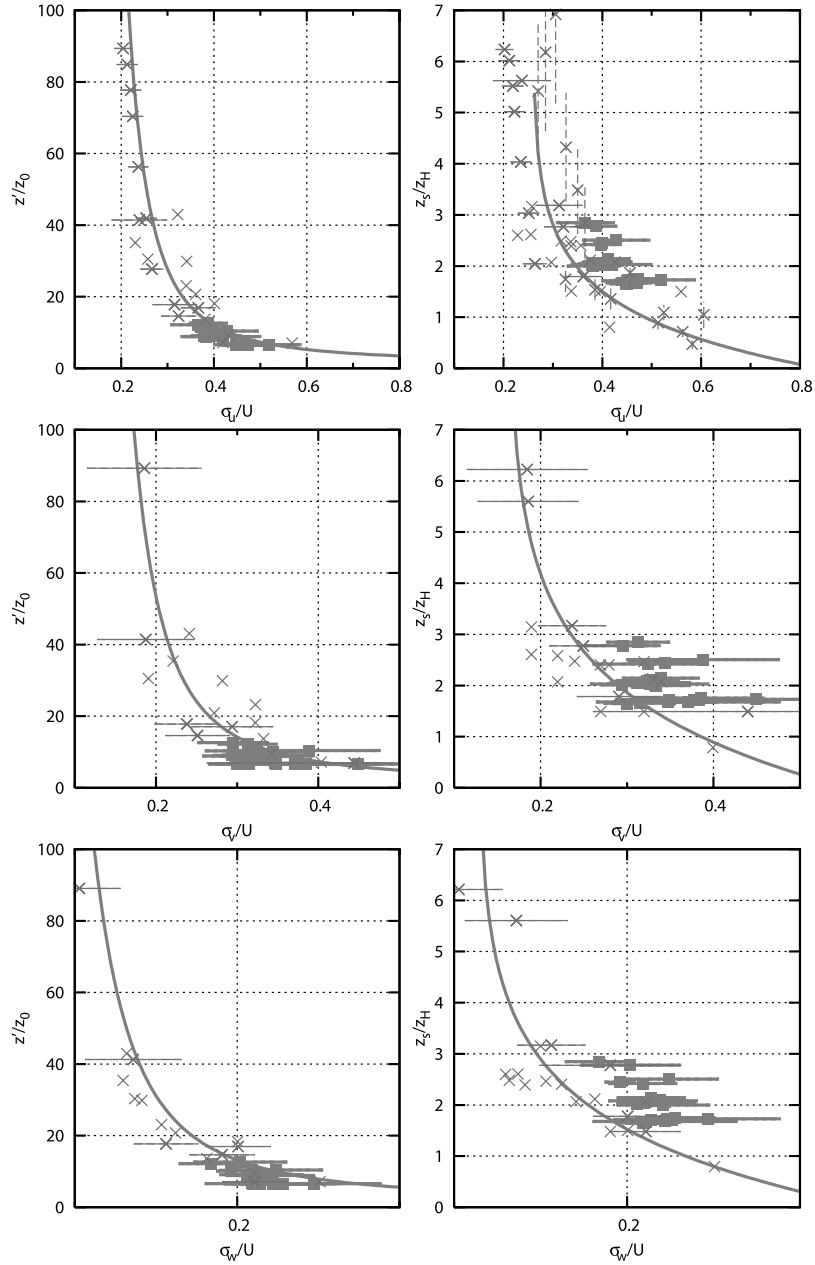

Figure 14. Turbulence intensities (top) $I_U = \sigma_u/U$, (middle) $I_v = \sigma_v/U$, and (bottom) $I_w = \sigma_w/U$ for neutral conditions with nondimensional heights z'/z_0 (left) and z_s/z_H (right). The lines in the left column are from *Roth* [2000] based on theory, his equation (8), and those in the right column are from his empirical equation (9), which has the form $I_i = a_i + b_i \exp[-c_i(z_s/z_H)]$ with coefficients for u of $a_i = 0.259$, $b_i = 0.582$, and $c_i = 0.943$; for v of 0.163, 0.391, and 0.563; and for w of 0.114, 0.226, and 0.634, respectively. See color version of this figure in the HTML.

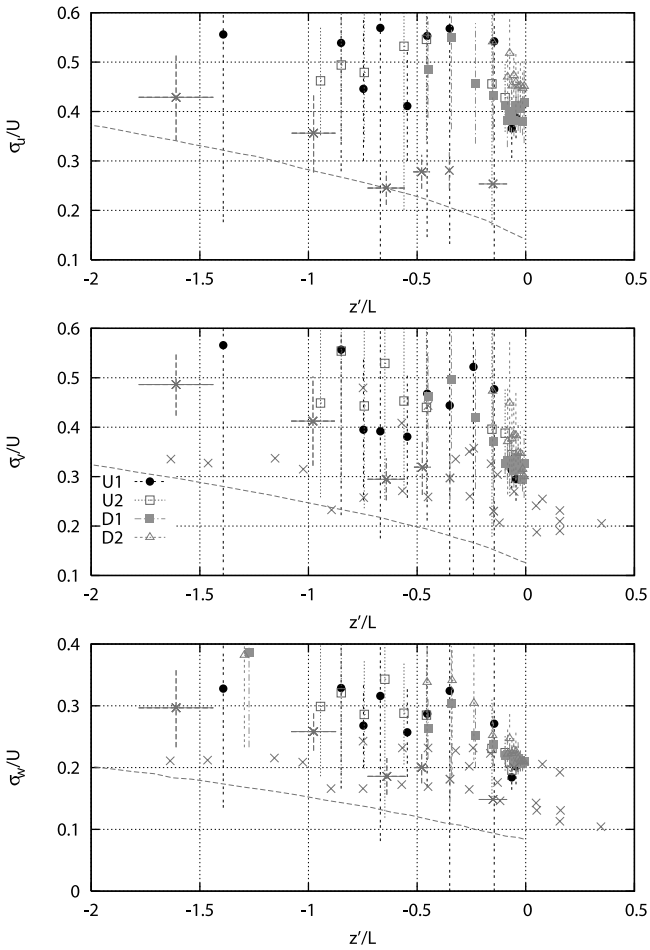

Figure 15. Turbulence intensity with stability with *Roth* [2000, Figure 8] data. See color version of this figure in the HTML.

urban data available, the new results provide further confirmation of the impact of dense urban areas on turbulent behavior.

[54] **Acknowledgments.** Funding for this project was provided by the National Science Foundation (BCS-0095284), Météo-France, ESCOMPTE, NSERC, and CFCAS (GR022). The project UBL/CLU-ESCOMPTE is funded by the CNRS programs for remote sensing from space (PNTS) and atmospheric dynamics (PATOM). We would like to thank the Cour Administrative d'Appel for providing the site and V. Anderson, B. Crawford, F. Cropley, M. Irvine, P. Jackson, J.-P. Lagouarde, V. Masson, J. Noilhan, S. Roberts, S. Scott, C. Souch, J. Voogt, and C. Walsh for their help in the field, with the preparation of equipment, and/or with data analyses. Information for the development of the surface database was provided by D. Groleau, N. Long, and M. A. Velay-Dabat. Paul Sabatier University (Toulouse, France) and CNRM provided funding for A.L.'s stay at Indiana University. We acknowledge helpful discussions with M. Kanda and D. Sailor regarding the role of anthropogenic heat in the energy balance.

References

Aida, M. (1982), Urban albedo as a function of the urban structure: A model experiment: 1, *Boundary Layer Meteorol.*, *23*(4), 405–413.

Anderson, D. E., and J. Taggart (2002), Urban ecosystem-atmosphere exchanges of carbon dioxide, paper presented at 4th Symposium on the Urban Environment, Am. Meteorol. Soc., Norfolk, Va.

Arnfield, A. J. (1982), An approach to the estimation of the surface radiative properties and radiation budgets of cities (Columbus, Ohio), *Phys. Geogr.*, *3*(2), 97–122.

Baldocchi, D., et al. (2001), FLUXNET: A new tool to study the temporal and spatial variability of ecosystem-scale carbon dioxide, water vapor, and energy flux densities, *Bull. Am. Meteorol. Soc.*, *82*(11), 2415–2434.

Christen, A., R. Vogt, M. W. Rotach, and E. Parlow (2002), First results from Bubble: Partitioning of turbulent heat fluxes and urban surfaces, paper presented at 4th Symposium on the Urban Environment, Am. Meteorol. Soc., Norfolk, Va.

Crawford, B., and C. S. B. Grimmond (2003), Investigations of anthropogenic heat flux: A physical model and real world estimations, in *Proceedings of the 5th International Conference on Urban Climate*, vol. 1, pp. 169–172, Int. Assoc. for Urban Clim., Bloomington, Indiana.

Cros, B., et al. (2004), The ESCOMPTE program: An overview, *Atmos. Res.*, *69*(3–4), 241–279.

Dabberdt, W. F., et al. (2004), Meteorological research needs for improved air quality forecasting: Report of the 11th Prospectus Development Team of the US Weather Research Program, *Bull. Am. Meteorol. Soc.*, *85*(4), 563–586.

Feigenwinter, C., R. Vogt, and E. Parlow (1999), Vertical structure of selected turbulence characteristics above an urban canopy, *Theor. Appl. Climatol.*, *62*(1–2), 51–63.

Finnigan, J. J., R. Clement, Y. Malhi, R. Leuning, and H. A. Cleugh (2003), A re-evaluation of long-term flux measurement techniques. Part I: Averaging and coordinate rotation, *Boundary Layer Meteorol.*, *107*(1), 1–48.

Grimmond, C. S. B. (1992), The suburban energy-balance: Methodological considerations and results for a midlatitude west-coast city under winter and spring conditions, *Int. J. Climatol.*, *12*(5), 481–497.

Grimmond, C. S. B., and T. R. Oke (1995), Comparison of heat fluxes from summertime observations in the suburbs of four North American cities, *J. Appl. Meteorol.*, *34*(4), 873–889.

Grimmond, C. S. B., and T. R. Oke (1999a), Aerodynamic properties of urban areas derived from analysis of surface form, *J. Appl. Meteorol.*, *38*(9), 1262–1292.

Grimmond, C. S. B., and T. R. Oke (1999b), Heat storage in urban areas: Local-scale observations and evaluation of a simple model, *J. Appl. Meteorol.*, *38*(7), 922–940.

Grimmond, C. S. B., and T. R. Oke (2002), Turbulent heat fluxes in urban areas: Observations and a Local-Scale Urban Meteorological Parameterization Scheme (LUMPS), *J. Appl. Meteorol.*, *41*(7), 792–810.

Grimmond, C. S. B., S. K. Potter, H. N. Zutter, and C. Souch (2001), Rapid methods to estimate sky-view factors applied to urban areas, *Int. J. Climatol.*, *21*(7), 903–913.

Grimmond, C. S. B., T. S. King, F. D. Cropley, D. J. Nowak, and C. Souch (2002a), Local-scale fluxes of carbon dioxide in urban environments: Methodological challenges and results from Chicago, *Environ. Pollut.*, *116*, S243–S254.

Grimmond, C. S. B., B. D. Offerle, J. Hom, and D. Golub (2002b), Observations of local-scale heat, water, momentum and CO_2 fluxes at Cub Hill, Baltimore, paper presented at 4th Symposium on the Urban Environment, Am. Meteorol. Soc., Norfolk, Va.

Harrison, R., B. McGoldrick, and C. G. B. Williams (1984), Artificial heat release from Greater London, 1971–1976, *Atmos. Environ.*, *18*(11), 2291–2304.

Ichinose, T., K. Shimodozono, and K. Hanaki (1999), Impact of anthropogenic heat on urban climate in Tokyo, *Atmos. Environ.*, *33*(24–25), 3897–3909.

Irvine, M., J.-P. Lagouarde, J.-M. Bonnefond, C. S. B. Grimmond, and T. R. Oke (2002), Spectral analyses of optical scintillation: Refraction and absorption components in an urban zone, paper presented at 4th Symposium on the Urban Environment, Am. Meteorol. Soc., Norfolk, Va.

Kaimal, J. C., and J. J. Finnigan (1994), *Atmospheric Boundary Layer Flows: Their Structure and Measurement*, 289 pp., Oxford Univ. Press, New York.

Kastner-Klein, P., and M. W. Rotach (2004), Mean flow and turbulence characteristics in an urban roughness sublayer, *Boundary Layer Meteorol.*, *111*(1), 55–84.

Kłysik, K. (1996), Spatial and seasonal distribution of anthropogenic heat emissions in Łódź, Poland, *Atmos. Environ.*, *30*(20), 3397–3404.

Lagouarde, J.-P., M. Irvine, J.-M. Bonnefond, C. S. B. Grimmond, N. Long, T. R. Oke, J. Salmond, and B. Offerle (2002), Sensible heat flux estimated over the city of Marseille, using a LAS scintillometer, paper presented at 4th Symposium on the Urban Environment, Am. Meteorol. Soc., Norfolk, Va.

Lagouarde, J.-P., M. Irvine, J.-M. Bonnefond, C. S. B. Grimmond, N. Long, T. R. Oke, J. Salmond, and B. Offerle (2004), Monitoring the sensible heat flux over urban areas using large aperture scintillometry: Case study of Marseille city during the ESCOMPTE experiment, *Boundary Layer Meteorol.*, in press.

Lee, X. H. (1998), On micrometeorological observations of surface-air exchange over tall vegetation, *Agric. For. Meteorol.*, *91*(1–2), 39–49.

Lemonsu, A., C. S. B. Grimmond, and V. Masson (2004a), Modelling the surface energy balance of an old Mediterranean city core, *J. Appl. Meteorol.*, *43*, 312–327.

Lemonsu, A., G. Pigeon, V. Masson, P. Durand, and F. Said (2004b), Sea-town interactions over Marseille. Part I: 3-D urban boundary layer structure, *Theor. Appl. Climatol.*, in press.

Long, N., P. G. Mestayer, and C. Kergomard (2002), Development of a software to describe the city morphology and to compute aerodynamic parameters from an urban data base, paper presented at 4th Symposium on Urban Environment, Am. Meteorol. Soc., Norfolk, Va.

Massman, W. J., and X. Lee (2002), Eddy covariance flux corrections and uncertainties in long-term studies of carbon and energy exchanges, *Agric. For. Meteorol.*, *113*(1–4), 121–144.

Mestayer, P., et al. (2004), The Urban Boundary Layer Field Campaign in Marseille (UBL/CLU-ESCOMPTE): Set-up and first results, *Boundary Layer Meteorol.*, in press.

Moriwaki, R., and M. Kanda (2004), Seasonal and diurnal fluxes of radiation, heat, water vapor and CO_2 over a suburban area, *J. Appl. Meteorol.*, in press.

National Climatic Data Center (2002), GSN datasets, http://lwf.ncdc.noaa.gov/oa/climate/gsn/gsndata.html, Asheville, N. C.

Nemitz, E., K. J. Hargreaves, A. G. McDonald, J. R. Dorsey, and D. Fowler (2002), Meteorological measurements of the urban heat budget and CO_2 emissions on a city scale, *Environ. Sci. Technol.*, *36*(14), 3139–3146.

Offerle, B., C. S. B. Grimmond, and T. R. Oke (2003), Parameterization of net all-wave radiation for urban areas, *J. Appl. Meteorol.*, *42*(8), 1157–1173.

Offerle, B., C. S. B. Grimmond, K. Fortuniak, K. Kłysik, and T. R. Oke (2004), Temporal variations in observed heat fluxes over a northern European downtown, *Theor. Appl. Climat.*, in press.

Oke, T. R. (1987), *Boundary Layer Climates*, 435 pp., Routledge, New York.

Oke, T. R. (1997), Urban environments, in *The Surface Climates of Canada*, edited by W. G. Bailey, T. R. Oke, and W. R. Rouse, pp. 303–327, McGill/Queens Univ. Press, Montreal.

Oke, T. R. (2004), Initial guidance to obtain representative meteorological observations at urban sites, *IOM Rep. 81.TD*, World Meteorol. Organ., Geneva, in press.

Oliphant, A. J., C. S. B. Grimmond, H. N. Zutter, H. P. Schmid, H. B. Su, S. L. Scott, B. Offerle, J. C. Randolph, and J. L. Ehman (2004), Heat storage and energy balance fluxes for a temperate deciduous forest, *Agric. For. Meteorol.*, *126*, 185–201.

Panofsky, H. A., and J. A. Dutton (1984), *Atmospheric Turbulence, Models and Methods for Engineering Applications*, 417 pp., John Wiley, Hoboken, N. J.

Pawlak, W., and K. Fortuniak (2003), Application of physical model to study effective albedo, in *Proceedings of the 5th International Conference on Urban Climate*, vol. 1, 233–236, Int. Assoc. for Urban Clim., Bloomington, Indiana.

Paw U, K. T., D. D. Baldocchi, T. P. Meyers, and K. B. Wilson (2000), Correction of eddy-covariance measurements incorporating both advective effects and density fluxes, *Boundary Layer Meteorol.*, *97*(3), 487–511.

Pigeon, G., A. Lemonsu, P. Durand, and V. Masson (2002), Urban surface network in Marseille: Network optimisation using numerical simulations and results, paper presented at 4th Symposium on the Urban Environment, Am. Meteorol. Soc., Norfolk, Va.

Pigeon, G., A. Lemonsu, V. Masson, and P. Durand (2003), Sea-town interactions over Marseille: Part II: Consequences on atmospheric structure near the surface, in *Proceedings of the 5th International Conference on Urban Climate*, vol. 1, pp. 435–438, Int. Assoc. for Urban Clim., Bloomington, Indiana.

Reifsnyder, W. E. (1967), Radiation geometry in the measurement and interpretation of the radiation balance: Computer program for the determination of view factors, *Agric. Meteorol.*, *4*, 255–280.

Roberts, S. M., T. R. Oke, J. A. Voogt, C. S. B. Grimmond, and A. Lemonsu (2003), Energy storage in a European city center, in *Proceedings of the 5th International Conference on Urban Climate*, vol. 1, pp. 241–244, Int. Assoc. for Urban Clim., Bloomington, Indiana.

Rotach, M. W. (1995), Profiles of turbulence statistics in and above an urban street canyon, *Atmos. Environ.*, *29*(13), 1473–1486.

Rotach, M. W. (1999), On the influence of the urban roughness sublayer on turbulence and dispersion, *Atmos. Environ.*, *33*(24–25), 4001–4008.

Rotach, M. W., B. Fisher, and M. Piringer (2002), COST 715 Workshop on Urban Boundary Layer Parameterizations, *Bull. Am. Meteorol. Soc.*, *83*(10), 1501–1504.

Roth, M. (2000), Review of atmospheric turbulence over cities, *Q. J. R. Meteorol. Soc.*, *126*(564), 941–990.

Rouse, W. R., D. Noad, and J. McCutcheon (1973), Radiation, temperature and atmospheric emissivities in a polluted urban atmosphere at Hamilton, Ontario, *J. Appl. Meteorol.*, *12*, 798–807.

Sailor, D. J., and L. Lu (2004), A top-down methodology for developing diurnal and seasonal anthropogenic heating profiles for urban areas, *Atmos Environ.*, *38*(17), 2737–2748.

Schmid, H. P. (1994), Source areas for scalars and scalar fluxes, *Boundary Layer Meteorol.*, *67*(3), 293–318.

Schmid, H. P., C. S. B. Grimmond, F. Cropley, B. Offerle, and H. B. Su (2000), Measurements of CO_2 and energy fluxes over a mixed hardwood forest in the mid-western United States, *Agric. For. Meteorol.*, *103*(4), 357–374.

Schotanus, P., F. T. M. Nieuwstadt, and H. A. R. Debruin (1983), Temperature-measurement with a sonic anemometer and its application to heat and moisture fluxes, *Boundary Layer Meteorol.*, *26*(1), 81–93.

Soegaard, H., and L. Moller-Jensen (2003), Towards a spatial CO_2 budget of a metropolitan region based on textural image classification and flux measurements, *Remote Sens. Environ.*, *87*(2–3), 283–294.

Soux, A., J. A. Voogt, and T. R. Oke (2004), A model to calculate what a remote sensor 'sees' of an urban surface, *Boundary Layer Meteorol.*, *111*(1), 109–132.

Spronken-Smith, R. A. (2002), Comparison of summer- and winter-time suburban energy fluxes in Christchurch, New Zealand, *Int. J. Climatol.*, *22*(8), 979–992.

Su, H. B., H. P. Schmid, C. S. B. Grimmond, C. S. Vogel, and A. J. Oliphant (2004), Spectral characteristics and correction of long-term eddy-covariance measurements over two mixed hardwood forests in non-flat terrain, *Boundary Layer Meteorol.*, *110*(2), 213–253.

Uitto, J. I., and A. K. Biswas (2000), *Water for Urban Areas: Challenges and Perspectives*, 245 pp., U. N. Univ. Press, New York.

Vogt, R., A. Christen, M. W. Rotach, M. Roth, and A. N. V. Satyanarayana (2004), Fluxes and profiles of CO_2 in the urban roughness sublayer, *Theor. Appl. Climatol.*, in press.

Webb, E. K., G. I. Pearman, and R. Leuning (1980), Correction of flux measurements for density effects due to heat and water-vapor transfer, *Q. J. R. Meteorol. Soc.*, *106*(447), 85–100.

White, J. M., F. D. Eaton, and A. H. Auer (1978), The net radiation budget of the St. Louis metropolitan area, *J. Appl. Meteorol.*, *17*, 593–599.

Wilczak, J. M., S. P. Oncley, and S. A. Stage (2001), Sonic anemometer tilt correction algorithms, *Boundary Layer Meteorol.*, *99*(1), 127–150.

Wilson, K., et al. (2002), Energy balance closure at FLUXNET sites, *Agric. For. Meteorol.*, *113*(1), 223–243.

C. S. B. Grimmond and B. Offerle, Atmospheric Science Program, Department of Geography, Indiana University, 701 E. Kirkwood Avenue, Bloomington, IN 47405, USA. (grimmon@indiana.edu)

A. Lemonsu, CNRM, Météo France, 42 av. Coriolis, F-31057 Toulouse Cedex, France.

T. R. Oke, Department of Geography, University of British Columbia, 1984 West Mall, Vancouver, BC, Canada V6T 1Z2.

J. A. Salmond, School of Geography, Earth and Environmental Sciences, University of Birmingham, Edgbaston, Birmingham B15 2TT, UK.